Green Synthesis of $La(OH)_3$ @Fe_3O_4@PC Nanocomposite for Removal of Phosphate from Wastewater

Bizuneh Seifu Damitie

A Thesis Submitted to the Department of Applied Chemistry

School of Applied Natural Science

Presented in Partial Fulfillment of the Requirements for the Degree of

Master of Science in Applied Chemistry (Industrial Chemistry)

Office of Graduate Studies

Adama Science and Technology University

November, 2022

Adama, Ethiopia

Green Synthesis of La $(OH)_3$@Fe_3O_4@PC Nanocomposite for Removal of Phosphate from Wastewater

Bizuneh Seifu Damitie

Advisor: Aschalew Tadesse (PhD)

A Thesis Submitted to the Department of Applied Chemistry

School of Applied Natural Science

Presented in Partial Fulfillment of the Requirements for the Degree of

Master of Science in Applied Chemistry (Industrial Chemistry)

Office of Graduate Studies

Adama Science and Technology University

November, 2022

Adama, Ethiopia

APPROVAL SHEET

I, the advisor of the thesis entitled "**Green Synthesis of La $(OH)_3$@Fe_3O_4@PC Nanocomposite for Removal of Phosphate from Wastewater**" and developed by **Bizuneh Seifu Damitie**; here by certify that the recommendation and suggestions made by the board of examiners are appropriately incorporated into the final version of the thesis.

Aschalew Tadesse (PhD)

_____	_____	_____
Major Supervisor	Signature	Date

We, the undersigned, members of the Board of Examiners of the thesis by Bizuneh Seifu Damitie have read and evaluated the thesis entitled **"Green Synthesis of La$(OH)_3$ @Fe_3O_4@PC Nanocomposite for Removal of Phosphate from Wastewater"** and examined the candidate during the open defense. This is, therefore, to certify that the thesis is accepted for partial fulfillment of the requirement of the degree of Master of Science in Applied Chemistry (Specialization in Industrial Chemistry).

_____	_____	_____
Chairperson	Signature	Date
_____	_____	_____
Internal Examiner	Signature	Date
_____	_____	_____
External Examiner	Signature	Date

Finally, approval and acceptance of the thesis are contingent upon submission of its final copy to the Office of Postgraduate Studies (OPGS) through the candidate's Department Graduate Council (DGC) and School Graduate Committee (SGC).

_____	_____	_____
Department Head	Signature	Date
_____	_____	_____
School Dean	Signature	Date
_____	_____	_____
Office of Postgraduate Studies, Dean	Signature	Date

DECLARATION

I hereby declare that this Master Thesis entitled **"Green Synthesis of La $(OH)_3$@Fe_3O_4@PC Nanocomposite for Removal of Phosphate from Wastewater"** is my original work. That is, it has not been submitted for the award of any academic degree, diploma or certificate in any other university. All sources of materials that are used for this thesis have been duly acknowledged through citation.

_____	_____	_____
Name of the student	Signature	Date

RECOMMENDATION

I, the advisor of this thesis, hereby certify that I have read the revised version of the thesis entitled **"Green Synthesis of $La(OH)_3@Fe_3O_4@PC$ Nanocomposite for Removal of Phosphate From Wastewater"** prepared under my guidance by **Bizuneh Seifu Damitie** submitted in partial fulfillment of the requirements for the degree of Master of Science in Applied Chemistry (Industrial Chemistry). Therefore, I recommend the submission of revised version of the thesis to the department following the applicable procedures.

Aschalew Tadesse (PhD)

_____	_____	_____
Major Advisor	Signature	Date

LIST OF ABREVIATIONS

ASTU	Adama Science and Technology University
BET	Brunauer–Emmett–Teller
DI	Deionized water
EU	European Union
FTIR	Fourier Transform Infrared
JCPDS	Joint Committee on Powder Diffraction Standards
LCFs	Lanthanum Carbon Fibers
LM	Lanthanum Materials
MNPs	Magnetite Nanoparticles
MPC	Magnetic Porous Carbon
NCs	Nanocomposites
NMOs	Nano metal oxides
NPs	Nanoparticles
PC	Porous Carbon
SEM	Scanning electron microscopy
TGA	Thermal gravimetric analysis
TP	Total Phosphorous
USEPA	United State Environmental Protection Agency
UV-VIS	Ultraviolet Visible Spectroscopy
WWTP	Wastewater Treatment Plant
XRD	X-ray diffraction

TABLE OF CONTENTS

LIST OF FIGURES

LIST OF TABLES

ABSTRACT

The removal of contaminants from wastewater is a major challenge in the area of water pollution. The removal of phosphorus (P) from wastewater is primarily to reduce the potential for eutrophication in receiving water, and common in many countries. Developing a highly efficient, environmentally friendly and selective adsorbent for phosphate removal is a major challenge these days. Lanthanum- based nanocomposites have attracted much attention for their efficiency and capacity in removing phosphate from water because La^{3+} ion has a strong affinity with oxygen-donor atoms from phosphate. In addition phosphate could easily desorb from Lanthanum- based nanocomposites due to the weak H-bonding interaction between phosphate and the H-bond acceptor groups on the surface of Lanthanum-based nanocomposites. This study developed $La(OH)_3@Fe_3O_4@PC$ nanocomposite by first preparing Fe_3O_4 NPs, $La(OH)_3$ NPs and porous carbon separately by using algae extract as reducing agent, and then combining these nanoparticles in a fixed ratio to remove phosphate from wastewater. The synthesized nanomaterials were characterized by FTIR, XRD, BET, TGA, and SEM for surface, and physicochemical characteristics. Performance of the nanocomposite was evaluated in terms of adsorption kinetics, adsorption isotherms, different solution pH values, dose, contact hour and regenerative ability. Using the optimized parameters the result revealed that, the adsorption efficiency of the composite decreased by increasing the pH of the solution, increased by increasing the adsorbent dose and contact time, and reached maximum at pH 5, adsorbent dose of 0.2g, contact time of 30 min, initial phosphate concentration of 50 mg/L at room temperature. The $La(OH)_3@Fe_3O_4@PC$ nanocomposite showed a 98.42% phosphate removal efficiency, an excellent phosphate removal capacity of 40.16 mg/g, and excellent reusability for six cycles. It was found that, in 30 min, 0.2 g/L dosage of the nanocomposite was able to reduce the phosphate from Adama Science and Technology University Wastewater Treatment Plant effluent from 3.729 mg/L to 0.05877 mg/L.

Keywords: Wastewater treatment, Pollutants, Adsorption, Desorption, Nanoadsorbents, Lanthanum-based nanocomposite, and Eutrophication

1. INTRODUCTION

1.1. Background of Study

Phosphorus (P), an essential nutrient widely found in aquatic environments, is highly required for the growth of living organisms and the normal functioning of ecosystems. It is a major component of fertilizer and an important element for biological growth for nucleic acid synthesis and energy. Phosphorus occurs in three compounds in natural waters: inorganic dissolved orthophosphate, dissolved organic phosphorus compounds and particulate phosphorus (bound in biomass or attached to particles) (Xie et al., 2014). According to the values of pKa_1 and pKa_2 of phosphoric acid (2.16 ,7.21), the dominating species are monovalent and divalent P as removed from the aqueous solution denoted as $H_2PO_4^-$ and HPO_4^{2-}. Since the pKa_3 of phosphoric acid is 12.3, the trivalent forms of PO_4^{3-} can be neglected in the adsorption operation (Awual, 2019 ; Zheng et al., 2021).

According to Bowes et al. study, the main sources of P entering rivers in UK are sewage effluent and agricultural run-off with up to 70% belonging to sewage discharges (Bowes et al., 2015). Municipal and industrial waste water are the main point sources for phosphate while run-off from agriculture is the dominant non-point source. A study indicates that 4 to 15 mg/L phosphate may be contained in municipal wastewater, whereas effluent from chemical industries such as detergent manufacturing and metal coating processes may contain 14 to 25 mg/L phosphate (Mekonnen et al., 2020). However, excessive phosphate emission to water bodies leads to eutrophication, which is responsible for water quality deterioration of 30–50% water resources all over the world, algal blooms, oxygen depletion and even aquatic ecosystem (Liu et al., 2020; Song et al., 2020). Eutrophication has been a global environmental problem in natural water, such as in lakes, marshes, and reservoirs (Y. Wang et al., 2021). Previous studies revealed that the acceptable total phosphorus concentrations in lakes and other confined water bodies should not exceed 0.03 mg/L P (Luo et al., 2021; Ahmed & Lo, 2020). The effluent limit of total phosphorus according to United State Environmental Protection Agency (USEPA) Clean Water Act is 0.5-0.8 mg/L (Abdul Salim et al., 2018). In recent years, great progress has been made in limiting P inputs from the point and non-point contaminant sources. Therefore, the removal of phosphate before discharge to receiving waters is crucial in controlling eutrophication.

A wide range of treatment technologies are available for removing phosphorus from wastewater, including chemical precipitation, biological phosphorus removal, and adsorption. However, chemical precipitation often suffers from high costs and sludge handling with low efficiency for trace level concentration of phosphate removal. Operational difficulties hinder the application of biological method for removal of phosphate at low concentration in water (Y. Chen et al., 2020). Adsorption is a preferable approach for phosphate removal due to its attractive advantages such as simple operation, high removal efficiency, and fast adsorption rate especially at low P concentrations (Sengupta & Pandit, 2011). Many inorganic and organic adsorbents, as well as industrial by-products and biological wastes have been tested for their efficiency in removing P from wastewater. The adsorbent materials should have high affinity and selectivity for phosphate, should show fast adsorption, high stability, and scale-up of production should be easy (Lu et al., 2021).

Lanthanum is one of the abundant and relatively inexpensive rare earth elements, and is considered to be environmentally friendly. Due to its specific affinity for phosphate and high potential in effectively removing phosphate, Lanthanum has received wide attention in phosphate removal (Rahman et al., 2021). Various lanthanum-based adsorbents have been prepared and investigated for P adsorption like $La(OH)_3$-loaded magnetic mesoporous nanospheres, mesoporous lanthanum hydroxide, zeolite/lanthanum hydroxide, lanthanum modified silica spheres, lanthanum hydroxide-doped activated carbon fibre, $La(OH)_3/Fe_3O_4$ nanocomposites, magnetic porous biochar supported $La(OH)_3$ and lanthanum hydroxide nanorods (Zhang et al., 2021; Dai et al., 2014; Huang et al., 2015; Xie et al., 2015). Huang et al. found that $La(OH)_3$-modified exfoliated vermiculite has an excellent adsorption selectivity, high removal rate and wide operating pH for phosphate adsorption (W. Y. Huang et al., 2014). La-based adsorbents have their own advantages. However most of these adsorbents are not easily separable and also used chemicals as reducing agent during synthesis (Song et al., 2020). Therefore, it is essential to develop an adsorbent that has high P adsorption capacity and excellent recyclability.

In this study, $La(OH)_3$ and Fe_3O_4 nanoparticles were synthesized by using aqueous extract of green algae as a reducing and capping agent. The synthesized Fe_3O_4 nanoparticles were decorated on porous carbon (PC) prepared from starch by calcination in the presence of sodium hydrogen carbonate. Then Lanthanum was loaded into the

synthesized magnetic porous carbon to form $La(OH)_3@Fe_3O_4@PC$ composite and applied to adsorb phosphate from wastewater. The efficiency of phosphate adsorption by the composite material was investigated by various physio chemical analyses.

1.2. Statement of the Problem

In several developing countries, including Ethiopia, rivers are sources of drinking water and for irrigation purpose. These water sources are stored in reservoirs before being treated. To reduce algal growth in the supply of drinking water, pre-treatment of phosphorous is necessary. Water may contain phosphate derived from contact with natural minerals or through pollution from an application of fertilizer, sewage and industrial wastes. The excessive use of phosphorous in households and in the agricultural sectors that leads to a significant subsequent discharge into water bodies resulted in an increased P concentration in the water, which in turn leads to algal growth and causing eutrophication. Eutrophication induces fast growth of plants and algae, depopulating aquatic species, deteriorating water quality and accelerating water scarcity. Studies have shown that even at trace level of around 0.02 mg/L, P can accelerate eutrophication and reducing P input is crucial in controlling eutrophication symptoms such as algal bloom in many lake ecosystems (Li et al., 2016; Bruun et al., 2021). According to one study, Gilgel Abay contribute more than 90 % of the inflow among more than 40 rivers feeding Lake Tana of Ethiopia. This river contains about 20 mg/L phosphate as the study shows (Taffese, et al., 2014). Other study shows that the average phosphate concentration in Lake Hawassa was found to be 6.56 mg/L (Lencha et al., 2021). In Adama science and technology university wastewater treatment plant, the treated wastewater contains 3.729 mg/L phosphate at the effluent during this study measurement which is beyond the standard value. Thus, it is essential to remove the dissolved P mainly found as phosphate from wastewater before discharge and reduces the concentration of P and prevents eutrophication. In recent time, adsorption using nanocomposite appears the most economical method because of its inexpensiveness, easy working principle, and high pollutant uptake capacities. This study present the synthesis of $La(OH)_3$ decorated magnetite (Fe_3O_4) nanocomposite on porous carbon by green and eco-friendly method as adsorbent to remove phosphate from wastewater.

1.3. Objectives

1.3.1. General objective

To synthesize and characterize $La(OH)_3@Fe_3O_4$ composite decorated on porous carbon for phosphate adsorption from wastewater.

1.3.2. Specific objectives

- To synthesis $La(OH)_3$ NPs, Fe_3O_4 NPs and $La(OH)_3@Fe_3O_4@PC$ nanocomposite through green synthesis method by using algae as reducing agent
- To characterize the synthesized nanocomposite by using different characterization techniques like XRD, FTIR, BET, SEM, and TGA/DTG
- To investigate the effect of pH, adsorbent dosage, contact time, and initial concentration on adsorption efficiency and removal capacity of phosphate by the synthesized composite
- To study the adsorption-desorption cycle of the synthesized adsorbent

1.4. Scope of the Study

The scope of this study was limited to the synthesis of $La(OH)_3$ NPs, Fe_3O_4 NPs and $La(OH)_3@Fe_3O_4$ composite decorated on PC through green synthesis method by using algae as reducing and capping agent. The synthesized nanocomposite was characterized by using XRD, FTIR, BET, TGA/DTG, and SEM techniques.

1.5. Significance of the Study

Excessive release of phosphate is one dominant factor for harmful algal blooms outbreak, which results in eutrophication risk. In general, accelerated eutrophication of surface water leads to problems with its use for fisheries (because of blooming and food web change), recreation, industry or drinking water because of the increased growth of undesirable algae/ cyanobacteria and aquatic weeds, and oxygen shortages. This study is expected to provide a method to remove phosphate from wastewater that poses serious environmental problems by using a simple, cost-effective, and environmentally friendly adsorption method. This method can be applicable and useful in different water treatment plants for removal of phosphate from wastewater before discharge to the environment. For researchers, it is important to do further study by expanding this investigation.

2. LITERATURE REVIEW

2.1. Wastewater

Increase in population, fast industrial development, commercial and agricultural activities have intensified the demand of water. Wastewater is produced in different ways like in household, restaurant and industrial activities. The source of wastewater plays an important role on its properties and treated processes. Domestic wastewater (house and restaurant wastewater) normally holds contaminants like vegetable materials, grease and scum detergents, and sediment (El-sayed, 2020). Industrial wastewater may contain toxic chemicals and metals, organic wastes, radioactive elements, great quantities of sediment, high temperature waste or acidic/basic waste while storm wastewater may include; oil, fuel, insecticides, herbicides and residual sediments as shown in Figure 1.

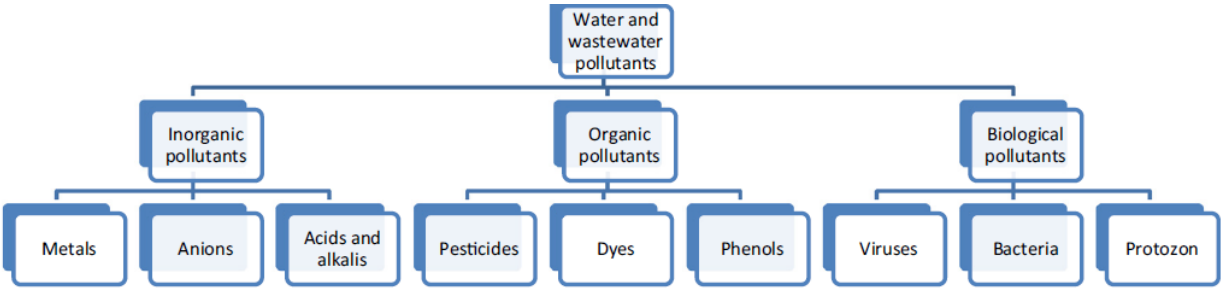

Figure 1: Water and wastewater contaminant types classified by their chemical nature (El-sayed, 2020)

Because of the scarcity of fresh water sources, the reuse of wastewater has become a smart choice for conserving and increasing the available water sources. The reuse of wastewater has numerous applications, including irrigation of agricultural soil, aquaculture, manufacturing consumptions, recreational and environmental practices, and artificial ground water recharge. Generally, wastewater may be reused for all purposes which fresh water is applied if an appropriate treatment is done to return it to water quality suitable for the intended application.

Several techniques have been reported for wastewater treatment which includes physical, chemical, and biological processes that are considered effective enough for water treatment in many ways. Adsorption is usually considered a cost effective and reliable method for wastewater treatment (El-sayed,2020). The removal efficiency of adsorption can range up to 99.9%. The United States Environmental Protection Agency (USEPA) declared the

adsorption process as one of the most excellent and best wastewater treatment techniques, among others (Rashid et al., 2021). Adsorption is basically a process of mass transfer in which solute or removable species are transported from a runny phase onto the surface phase. By physiochemical interactions, adsorbed species are bounded to the solid surface (Manchisi et al., 2020).

2.2. Nanoparticles

Nanoparticles (NPs) are the products of nanotechnology usually ranging in size from 1 to 100 nm and have been classified on the basis of origin, dimensions, and structural configurations (Vikrant & Kim, 2018).These particles are transients between bulk materials and molecular structures with a high ratio of surface area to mass. Anthropogenic inorganic nanoparticles (metallic nanoparticles) possessing extremely small size and large surface to volume ratio have unique properties, such as magnetic and optical polarizability, electrical and thermal conductivity that have led to many applications with great scientific impetus as well as industrial significance. Noble metallic nanoparticles have significant utility in diverse fields, such as clinical diagnostics and therapeutics, electronics, cosmetics, textiles, food processing and packaging, wastewater treatment, environmental remediation and agriculture (Chaudhary et al., 2020).

Due to unique morphological (shape, size, and charge distribution) and physico-chemical properties of NPs, they find applications in almost every discipline of science, like space, energy, defense, communication, biomedicine, and agriculture. Use of NPs in disease diagnosis, imaging, treatment, drug delivery, tissue engineering, and cancer therapeutics is also increasing tremendously (Macys, 2005). However, application of NPs in biological entities, especially humans, is very critical, and the NPs used in biomedical applications should preferably be from green sources. Taking into consideration various factors, such as biocompatibility, bioavailability, bio-distribution, and most importantly biosafety of NPs, the current trend of synthesis of NPs is moving towards the safer side. NPs are mostly synthesized by physical and chemical methods such laser ablation, mechanical milling, electro explosion, and sol-gel, but they are hazardous for environmental and human health (Cheng et al., 2016). The trend to synthesize NPs from alternative, environmentally safe, cost-effective, and non-toxic green methods is increasing.

Green nanotechnology focuses on production of NPs using minimal or negligible toxic substances, while posing no damage to the environment and risk on human health. In these environment-friendly methods, biological systems such as bacteria, viruses, algae, yeast, fungi and plants have been widely used, leading to significant contributions to nanotechnology for green synthesis of NPs that are free from impurities. These biological systems possess various biological entities which behave as both reducing and capping agents in NP generation, either intracellular or extracellular (Sinha et al., 2015). Proteins, peptides, and functional groups (carbonyl, thiol, hydroxyl, and amine) present in biological entities reduce precursor salt into NPs called reducing or stabilizing agents. They cap and stabilize NPs at the same time; hence this type of synthesis is relatively simple, reproducible, and stable. The biosynthesis of NPs can be controlled by various physical factors, such as pH, concentration of metal precursor and bio-extract, contact time of reaction mixture, exposure to any light source, and temperature. These factors control the nucleation, growth, aging, agglomeration, and stabilization of NPs, which in turn can alter the size, shape, and crystallinity of the synthesized NPs (Chaudhary et al., 2020).

Interestingly, an emerging trend of studies related to the biosynthesis of metallic nanoparticles using algal species has been observed in the recent decade. Algae are a very diverse group of autotrophic unicellular or multicellular organisms that can be catalogued as microalgae (microscopic) and macroalgae (macroscopic) found in very diverse habitats. Various types of algae have been extensively explored as a potential tool for green synthesis of metallic nanoparticles at higher rate, probably due to their high capacity of metal accumulation. Recently, synthesis of metal nanoparticles using algae has attracted much attention due to their simplicity and cost effectiveness in terms of mass production as well as downstream processing of nanoparticles and environmental benignity; they greatly reduce the need for hazardous chemicals. Moreover, many algae have thick, rigid cell walls made up of polysaccharide and glycoprotein matrices containing several functional groups such as hydroxyl, carbonyl, carboxyl, thiol, sulfonate and amino and amidic groups (KuyucakandVolesky1989) which play a major role in metal reduction and accumulation. This means that polysaccharides and glycoproteins present in the algal cell wall are involved in bio-reduction and capping (Sharma et al., 2016).

Magnetic nanoparticles (MNPs), falling under the class of nanoparticles, ordinarily constitute of elements like iron, nickel and cobalt so they can be regimented using external magnetic field. Another reason is that they can be engaged for circumstantial purposes on the cornerstone of their biocompatibility, magnetic susceptibility, synthesis mode and characterization methods. MNPs have always proved to be serviceable not only in environmental redress but also in biomedical field involving cancer therapy, Alzheimer treatment, antimicrobial activities, targeted drug delivery and diagnostic applications (Zhou et al., 2015).

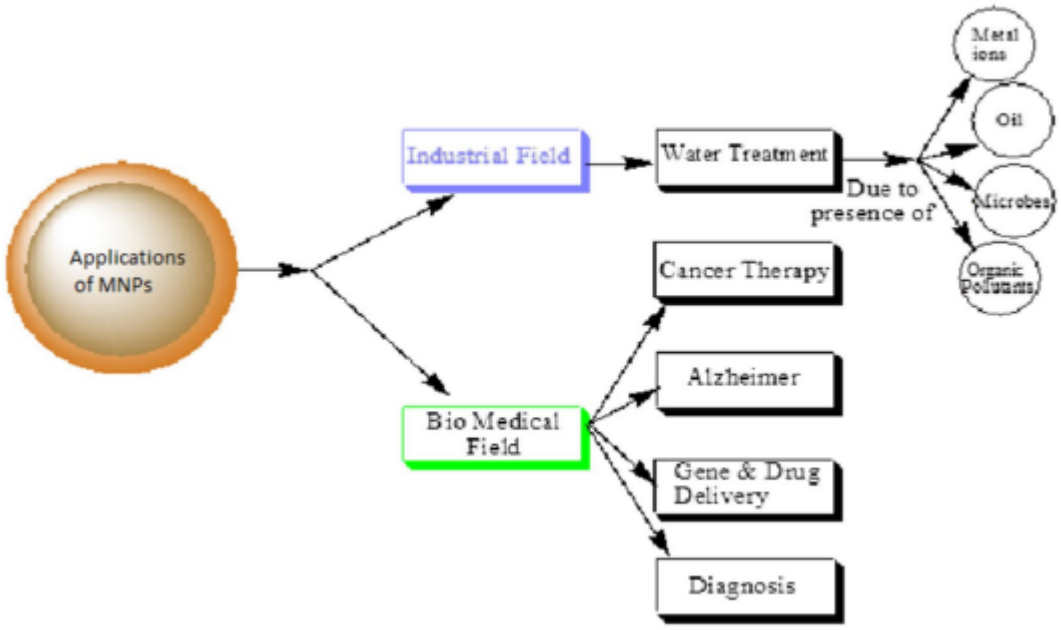

Figure 2: Applications of MNPs in industrial and biomedical field (Gupta et al., 2018).

2.2.1. Methods of synthesis

2.2.1.1. Chemical synthesis

In the last decade, highly stable, shape controlled and mono-dispersed MNPs have been generated using synthetic methods. The structure and morphology of the MNPs rely upon the method used for their synthesis which in turn greatly influences their magnetic properties. Consequently, various methods are proposed which include sol–gel, hydrothermal, co-precipitation, sonochemical, microemulsion, thermal decomposition and many more which can be directed to synthesize MNPs of different vital properties (Gupta et al., 2018).

2.2.1.2. Green synthesis

Now a day, synthetic methods to produce substances have been replaced by green chemistry. It has drawn a great attention of researchers because of its environment benign nature. Green chemistry makes use of non-toxic substances like plants tissues, plants extracts, micro-organisms, fruits, marine algae for synthesizing (Nayak et al., 2015). When substances are derived using green chemistry, the method is termed as green synthesis. It plays a great role in production of well-characterized (well sized and free from contamination) MNPs without compromising with nature. Plant extracts seem to be most appropriate among all candidates used in green synthesis for massive production of MNPs. In the synthesis, they act as reducing as well as stabilizing agent (Z. Wang et al., 2015). The choice of plant extract influences features of MNPs formed because different extracts possess different properties (concentration and combination of organic reducing agent). Metal ions are reduced to MNPs using biomolecules present in the plant extracts or plant tissues with much easiness (Anuradha et al., 2015). This biogenic synthesis is not only an effective process on account of providing high synthesis rate, stability, environmental amiability and facile reaction conditions (room temperature and pressure) but also an economical one if compared with relatively expensive chemical methods. Biosynthetic routes, though relatively complex, are more efficient than synthetic ones in way of providing required nanoscale and morphology (Gupta et al., 2018).

2.3. Nanoadsorbents for Wastewater Treatment

Nanotechnology allows the development of novel high-tech materials for more efficient water and wastewater remediation methods, such as membranes, adsorption materials, nanocatalysts, functionalized surfaces, coatings, and reagents. However, nano-adsorbent materials are considered the most suitable water and wastewater remediation methodology because of it's easy to apply and there is a wide range of adsorbents (Basheer, 2018). Nanomaterials show great promise as the best feasible way to treat organic as well as inorganic contaminants because of their unique properties such as high surface area and high adsorption capacity. In addition, the interaction between nanoadsorbents and contaminates may be chemisorption or physisorption depending on the functionalization of nanomaterial (Vikrant & Kim, 2018, El-sayed, 2020).

Adsorption is a surface phenomenon and widely used mechanism for the elimination of all types of pollutants. The adsorption process depends on the interaction between an absorbable solute and a solid adsorbent which has a highly porous surface structure. The attractive forces between the solute and the adsorbent cause the solute molecules to be concentrated on the adsorbent surface. The adsorption process leads to increasing the concentration of the adsorbate on the adsorbent surface. Adsorption is considered a very appropriate technique for wastewater purification due to its high efficiency, cost-effectiveness, versatility, and easy control (Gusain et al., 2020). The nature of an adsorbent is a very important factor in adsorption process where the adsorbent determines the efficiency, versatility and economics of the adsorption method. The three types of adsorption method are classified by the nature of the surface attachment which can be physical, chemical or exchange adsorption (El-sayed,2020).

Physical adsorption (Physisorption) is caused by Vander Waals forces and is the easiest to separate because these forces are weak in nature and it is essentially reversible. **Chemical adsorption** (Chemisorption) takes place through chemical bonding between adsorbate and adsorbent. Chemisorption happens only as a monolayer. In addition, materials that chemisorbed on solid surface are difficult to remove. It is principally irreversible.

Exchange adsorption is caused by the charge attraction between adsorbate and the surface. The shape and the morphology of nano-adsorbent materials also plays very important role in its properties and efficiency. These chemical and physical characteristics led to increasing their application as adsorbents compared to traditional adsorbents (Gatoo et al., 2014).

Because of their high porosity, small size, and active surface, nanoadsorbents not only are capable of removing contaminants with varying molecular size, hydrophobicity, and speciation behaviour, but also enable manufacturing process to consume raw materials efficiently without releasing its toxic adsorbed substance (Cheriyamundath & Vavilala, 2021). Nano adsorbents not only work rapidly, but also have considerable pollutant-binding capacities. They can also be chemically regenerated after being used (Fu et al., 2018). At the nanoscale, materials show unique characteristics and, because of their small size, they possess a large surface area and surface area to volume ratio. These characteristics improve the adsorption capacity of the nanoparticles. In addition to the large surface area, these particles show unique characteristics, such as catalytic potential and high reactivity, which make them

as better adsorbing materials than conventional materials. Because of their high surface area, nanoparticles have a greater number of active sites for interaction with different chemical species (Fu et al., 2018). Nanoadsorbents have nanoscale pores, high selectivity, high surface area, high permeability, good mechanical stability and good thermal stability (El-sayed, 2020).

Various types of adsorbents such as biomass, activated carbon, clays composite and metal oxide nanoparticles have been explored to remove phosphate from water. Among the various adsorbents, hybrid materials created by doping metal oxide nanoparticles into different host materials have demonstrated high phosphate selectivity via ligand exchange (inner-sphere complexation) between phosphate and the metal oxide nanoparticles (H. Dong et al., 2020). With regards to important operational parameters in the treatment of sewage, the efficiency of the removal of phosphate is highly dependent on the initial concentration of phosphate, adsorbent dosage and reaction time (Fang et al., 2017). As for the adsorption technique, the adsorbents play a key role in terms of adsorption capacity, removal rate, and selectivity. Removal capacity strongly depends upon the chemical composition and properties of metal oxides, like surface area, active sites and composite formation. The properties of metal oxide can also be adjusted by changing the synthesis conditions like changing the aging temperature, concentration of the metal salt, amount of precipitating agent, and annealing temperature (Ahmad et al., 2019).

In recent years, metal-based adsorption materials have been widely used for phosphate removal in wastewater such as hydrous zirconia-modified zeolite, magnesium oxide-enriched biochar and hydroxyl iron-aluminum pillared bentonites (Fang et al., 2018). Most of these adsorption materials have exhibited high adsorption selectivity and capacity for phosphorus but effective when the initial concentration of phosphorus is over 20 mg/L, which does not represent the characteristic of real contaminated water. In general, the phosphorus concentration of wastewater treatment plants effluents is under a certain level (10 mg P/L) (Zheng et al., 2021). Among different types of oxides and hydroxides of metals tested, those of Fe, Al, La and Ca have been regarded as effective adsorbents for the removal of phosphate due to their high phosphate binding capacity (Zheng et al., 2021). Hydrated metal oxides and hydroxides such as zirconium oxide, iron oxide, aluminum oxide and lanthanum oxide have

been immobilized into adsorbents to improve the surface and adsorption efficiency (P. Wang et al., 2019). In particular, lanthanide-based nanomaterials are often considered as efficient and promising candidates for phosphorus removal.

Lanthanum (La) is a trivalent metal and has hard Lewis acid property. Thus, it exhibits strong ligand adsorption for phosphate which behaves as a Lewis base. La has a good binding capacity to phosphate and an especially low solubility product in a complex system containing lanthanum phosphate, which has been employed as phosphate adsorbents. Moreover, La could provide more coordination sites and shows excellent sensitivity to phosphorus even at micro levels (Liu et al., 2020). Due to its hard Lewis acid property, Lanthanum compounds like La_2O_3 and $La(OH)_3$ are considered as electron pair acceptors and have ultra-strong affinity toward phosphate as Lewis base (Zheng et al., 2021). Up to know a variety of La-based materials have been developed to remove phosphate from wastewater by choosing suitable host to support La for an improved efficiency. Host materials with high specific surface area, such as carboxylate multi-walled carbon nanotubes, graphene, and mesoporous hollow silica spheres can support a good amount of La and thus, can lead to impressive phosphate adsorption capacity. However, most of these materials are limited by high cost and subsequent difficulties in their separation from treated water, which hinder their large-scale application (Fang et al., 2018).

A combination of La onto the support materials enhances both adsorption kinetics and capture capacity. Various La-loaded porous adsorbent such as La loaded mesoporous silica, porous lanthanum, biochar/lanthanum, graphene/lanthanum, La-loaded activated fiber and La-loaded zeolite have been proven to be favorable for improving phosphate uptake capacity(Lin & Chen, 2021). Many of these hybrid sorbents suffered an unsatisfactory sorption performance due to the lower amounts of La load in composites. The maximum phosphate sorption capacity observed for La-modified bentonite and La-Carbon fibers respectively are 14.0 and 20.51 mg P/g, which might influence their phosphate removal and recovery potential (Shan et al., 2020). In addition, the separation of spent La-based materials (especially for powdered sorbents) from treated effluents remains an issue. Once used, lanthanum-based materials are difficult to separate and recover from river water. Traditional methods like Filtration and sedimentation may be ways to recover the used adsorbent, but these methods

consume a lot of energy and subject to problems such as filter blockage, increasing their costs (Ahmed & Lo, 2020). Enhancing the separability of La-based materials by incorporation of magnetic materials is gaining significant interest. For example, Lai et al. developed a core/shell $Fe_3O_4/SiO_2/La(OH)_3$ magnetic composite, which showed an adsorption capacity toward phosphate of 27.8 mg P/g and could be easily separated through magnetic separation (Lai et al., 2016). Wu et al. synthesized novel La $(OH)_3/Fe_3O_4$ nanocomposites, which also showed good adsorption capacity and magnetic separability (Ahmed & Lo, 2020).

2.4. Magnetic Porous Carbon (MPC)

Carbon-based adsorbents possess large surface areas and abundant pore structures and have shown great potential in the removal of undesirable organic pollutants from aqueous solutions (Zhouetal.,2012).Recently,magneticcarboncompositeshavebeendevelopedand are not only high efficiency adsorbents for removal of pollutants from aqueous solutions, but are also easily collected magnetically after adsorption (Zhang et al.,2012).The introduction of a magnetic medium(such as maghemite,γ-Fe_2O_3) to carbon-based adsorbents by a pyrolysis activation(simultaneous activation and magnetization) or chemical co-precipitation reaction is an efficient method to enable the adsorbent to be efficiently separated with an external magnetic field. However, for a low surface area of carbonaceous material, co-precipitation reaction is not an efficient and facile method due to its negative effect on porosity of products (Oliveira et al., 2002). But, both an enhanced surface area and excellent magnetization property can be simultaneously obtained via pyrolysis activation (Zhang et al., 2012). However, few studies were presented to develop this promising technology for the preparation of MPC (Zhu et al., 2014).

Although NPCs perform as good adsorbents, it is difficult to separate NPCs from aqueous solution, thus limiting their applications in this field. Introducing magnetic particles into NPCs can enlarge the scope of applications, especially for adding magnetic functionality to realize magnetic separation. Many kinds of procedures were used for generating such magnetic nanoporous carbon materials, including hydrothermal methods, co-casting methods, template carbonization, and thermal treatment of organometallic compounds (J. D. Xiao et al., 2013).

2.5. La $(OH)_3/Fe_3O_4$ Nanocomposites

Nano metal oxides (NMOs) show an effective and specific adsorption towards various aquatic pollutants. However, they are usually present as fine or ultrafine particles, which often lead to problems such as activity loss due to agglomeration, difficult separation, and excessive pressure drops when applied in flow-through systems (Fu et al., 2018). An effective approach to overcome this technical obstacle is to fabricate hybrid adsorbents by coating nanoparticles into/onto porous supports of larger size. Fe_3O_4 nanoparticles can be coated with inorganic material such as silica, gold or silver. These coatings not only improve the stability of the nanoparticles in solution but also provide sites for covalent binding with specific ligands to the nanoparticle surface. The use of silica provides great stability to the nanoparticles dispersion against changing of pH and concentration of electrolytes (Carlos et al., 2013). Lanthanum (La) has a good binding capacity to phosphate and an especially low solubility product in a complex system containing lanthanum phosphate, which has been employed as phosphate adsorbents. Moreover, La could provide more coordination sites and shows excellent sensitivity to phosphorus even at micro levels. Hence a combination of La onto the support materials enhances both adsorption kinetics and capture capacity (X. Xiao et al., 2014). However, the adsorption materials containing higher lanthanum loading usually exhibited significant amounts of lanthanum leachate in solution during the phosphorus adsorption process, and the La usage efficiency was lower. It is of great significance to develop a porous and environmental-friendly support for lanthanum deposition that could promote the removal of relatively low-level P and improve the lanthanum utilization efficiency (Zheng et al., 2021). The incorporation of lanthanum can significantly increase both the retention capacity and the adsorption kinetics of natural adsorbents like clays. The lanthanum phosphate compound, known as “Rhabdophane”, is a highly insoluble salt in water (Kuroki et al., 2014).

La^{3+}, La_2O_3(s) and $La(OH)_3$(s) are common sources of La ions when non-La carriers are transformed into La-based materials (B. Wu et al., 2017). During synthesis, La^{3+} is incorporated into the structure of a carrier by exchange with Ca^{2+} or Na^{+} whereas La_2O_3(s) and $La(OH)_3$ (s) are incorporated into the carriers by way of co-calcination , co-precipitation , calcination or precipitation of material preloaded with La^{3+} under alkaline conditions (Zhi et

al., 2020). Carrier materials with internal and surface structures (e.g., porous structures with relatively high specific surface areas) are often selected to facilitate La access to phosphate and enhance La dispersion to promote the crystallization of $LaPO_4$. Many materials, such as silica spheres (W. Huang et al., 2015), porous zeolite (He et al., 2017), and magnetic mesoporous nanospheres (L. Chen et al., 2019), have been investigated as a supporter for La oxides or hydroxides. In previous literature, one gram La_2O_3 modified oak takes up 46.37 mg phosphorus (Wang et al., 2016), and $La(OH)_3$-modified magnetic pineapple biochar absorbs 101.16 mg/g (Ahmed & Lo, 2020). To evenly distribute La over the surface, the preferred supporting materials should have large surface areas and abundant pores. Other material design factors include enhancing the affinity of phosphate for surface adsorption, such as an overall positive charge of the carrier as characterized by the point of zero charge (Ahmed & Lo, 2020).

The increased solubility of Lanthanum can occur under some environmental conditions including at moderately acidic pH values (pH < 4.5), highly saline conditions, and in the presence of organic matter (Razanajatovo et al., 2021). At the same time, dissolved Lanthanum will likely undergo hydrolysis, bind to organic matter, and combine with phosphate to precipitate Rhabdophane ($LaPO_4 \cdot H_2O$), all of which reduce the bioavailability of Lanthanum in aquatic environments (Zhi et al., 2020). Therefore, lanthanum has often been preferred as a loading agent to enhance the removal of phosphate from aqueous solutions. Lanthanum hydroxides are attractive adsorbents due to multiple merits including low toxicity, high chemical stability and biocompatibility. Besides, lanthanum-based adsorbents are promising candidates for phosphate removal due to a high adsorption capacity, wide operating pH range and high removal rate (Zong et al., 2018). Many lanthanum-based adsorbents including porous lanthanum, biochar/lanthanum and graphene/lanthanum have been developed to improve the removal of phosphate from wastewater (Fang et al., 2018). Hence, a combination of La onto the support materials enhances both adsorption kinetics and capture capacity. Some nano-sized materials may require a supporting matrix or modification with Fe_3O_4 for magnetic separation. A study showed that magnetite nanoparticles have a limited adsorption capacity while a La –decorated magnetite showed a significantly enhanced adsorption capacity for phosphate (Fu et al., 2018). One of such types of adsorbents is La

$(OH)_3/Fe_3O_4$ composite. The main benefits of La $(OH)_3$ /Fe_3O_4 composites for phosphate removal are their ability to strongly bind phosphate under diverse environmental conditions (e.g., over a wide pH range, in the presence of diverse aqueous constituents) and excellent selectivity (W. Y. Huang et al., 2014). The maximum phosphate uptake capacity of $La(OH)_3/Fe_3O_4$ composites correlates primarily with the La content of $La(OH)_3/Fe_3O_4$ composites, whereas reaction kinetics are influenced by $La(OH)_3/Fe_3O_4$ composites, formulation and ambient environmental conditions (e.g. pH, presence of coexisting ions, ligands, organic matter) (Song et al., 2020).

The higher phosphate adsorption capacity of $La(OH)_3/Fe_3O_4$ to other La-based sorbents could be understood from the differences in the contents of active sites (i.e., La) that are responsible for phosphate uptake, the density of surface hydroxyl groups on the active sites, and the surface charge on the adsorbent surface. The $La(OH)_3/Fe_3O_4$ has La content of 27.8%, which is much higher than that of $Fe_3O_4@SiO_2@La_2O_3$ (11.2%) and is comparable to $La(OH)_3$-modified exfoliated vermiculites (31.2%) (W. Y. Huang et al., 2014). Higher La content leads to higher phosphate adsorption capacity, as La mainly serves as active sites for phosphate adsorption. In addition, phosphate uptake by La-based adsorbents has been shown to occur through ligand exchange at surface hydroxyl sites and electrostatic attraction (Zheng et al., 2021).

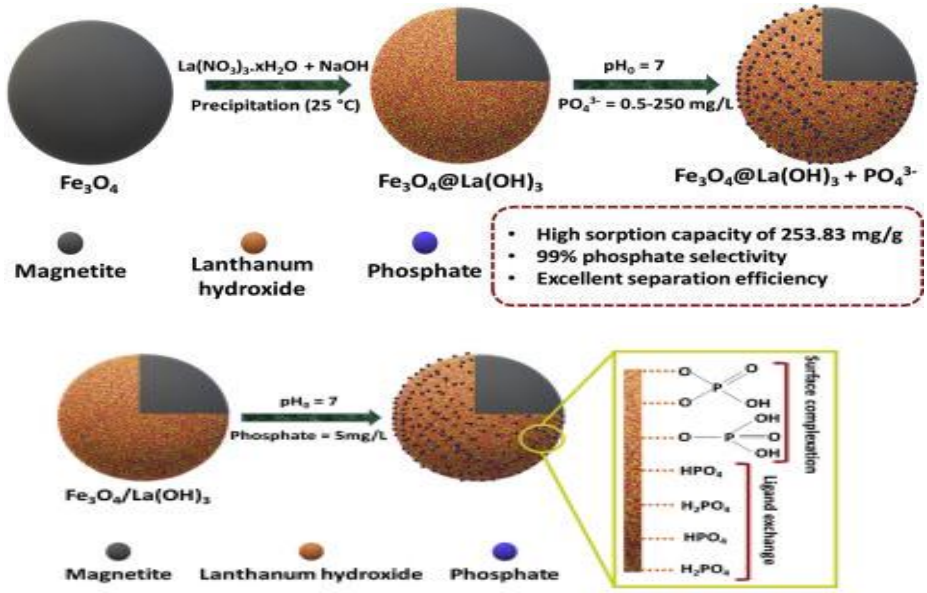

Figure 3: Schematic illustration of the phosphate sorption mechanism on the Fe_3O_4/ $La(OH)_3$ composite (Ahmed & Lo, 2020).

It has been speculated that mechanisms of phosphate adsorption by La-based materials include electrostatic interactions (S. Dong et al., 2017), ion exchange (Xie et al., 2014), ligand exchange (L. Zhang et al., 2012 ;S. Dong et al., 2017), Lewis acid-base interactions (L. Zhang et al., 2012), and inner-sphere complexation (W. Wu & Maravelias, 2019). Mostly, ligand exchange and electrostatic attractions are the main mechanisms that jointly facilitated the adsorption of phosphate (Fu et al., 2018).

2.6. Kinetics of Adsorption

Adsorption is one of the most widely applied techniques for pollutant removal from contaminated media. When adsorption is concerned, thermodynamic and kinetic aspects should be involved to know more details about its performance and mechanisms. Kinetic performance of a given adsorbent provides great significance for the pilot application. Adsorption kinetics is the measure of the adsorption uptake with respect to time at a constant pressure or concentration and is employed to measure the diffusion of adsorbate in the pores. From the kinetic analysis, the solute uptake rate, which determines the residence time required for completion of adsorption reaction, may be established. Also, one can know the scale of an adsorption apparatus based on the kinetic information (Qiu et al., 2009). Kinetics study helps to select optimum operating conditions for the full-scale batch process, which have been applicable to investigate the mechanism of adsorption and potential rate-controlling steps. Kinetic parameters are significant for the prediction of adsorption rate, and give useful information for designing and modeling the adsorption processes (Batool et al., 2018). Several kinetic models such as the pseudo first- and second-order equations, intra-particle diffusion and Elovich equations are used to interpret the time dependent experimental data and examine the controlling mechanism of adsorption process (Rodrigues and Silva, 2009; Chen et al., 2007).

2.6.1. Pseudo-first-order model

The first-order model is believed to be the earliest model and it was developed by Lagragren in 1898 (Qiu et al., 2009). To describe the kinetic process of liquid-solid phase adsorption, it is generally used in the form proposed by Ho and McKay as:-

$$Log(qe - qt) = -\frac{K_1}{2.303}t + Logqe \quad (1)$$

Where q_e and q_t (mg/g) are the adsorption capacities at equilibrium and at a time t (min), respectively, K_1 (min^{-1}) is the pseudo first order rate constant for the kinetic model (Y. Wang et al., 2021).

2.6.2. Pseudo-second-order model

It was not very popular until 1999 when Ho and McKay analyzed a number of experimental results taken from the literature, and arrived at the conclusion that, "for all of the systems studied, the pseudo-second order reaction kinetics provide the best correlation of the experimental data" (Simonin, 2016). Currently, the pseudo-second-order rate equation, popularized by Ho and McKay, is probably the most widely used model for adsorption kinetics. Most of the time this equation is used when the first-order model fails and the equation for this model is written as:-

$$\frac{t}{qt} = \frac{1}{K_2 qe^2} + \frac{1}{qe}t \qquad (2)$$

where q_e(mg/g) is the adsorption capacities at equilibrium; K_2(g/(mg min)) is the equilibrium rate constant of pseudo-second order adsorption (W. Y. Huang et al., 2014;S. J. Liu et al., 2016;Song et al., 2020).

2.7. Adsorption Isotherm Models

Adsorption isotherms have been of great importance to research dealing with environmental protection and adsorption techniques. An adsorption isotherm is a graph that represents the variation in the amount of adsorbate adsorbed on the surface of the adsorbent with the change in pressure at a constant temperature. The adsorption isotherm experiments were used to determine the maximum phosphate adsorption capacities of the adsorbent. It the most suitable way to evaluate the adsorption process as well as to understand the interrelation between the amounts of adsorbate on the adsorbent surface to its concentration (Ayawei et al., 2017). The adsorption isotherm models are used to describe the phenomenon governing the retention or release of a substance from the aqueous porous media or aquatic environments to a solid phase at a constant temperature and pH. Among numerous isotherm models, Langmuir and Freundlich isotherm models are most widely used models to describe the single-solute adsorption because of the corresponding simple mathematical forms and excellent fitting performance (Hu & Zhang, 2019).

In this study, Langmuir and Freundlich models were used to fit the isotherms data for the adsorption of phosphate at pH = 5 and room temperature for assessing the adsorption behavior of the adsorbents.

2.7.1. Langmuir adsorption isotherm model

The Langmuir adsorption isotherm is used to describe the equilibrium between adsorbate and adsorbent system, where the adsorbate adsorption is limited to one molecular layer at or before a relative pressure of unity is reached. The isotherm initially proposed by Langmuir in 1918 is generally suitable for describing the chemisorption process when ionic or covalent chemical bonds are formed between the adsorbent and the adsorbate. The Langmuir adsorption isotherm describes the surface as homogeneous, assuming that there is no lateral interaction between adjacent adsorbed molecules when a single molecule occupies a single surface site. Langmuir adsorption isotherms are based on the assumption that the reactive groups are homogeneously distributed over the particulate's surface and that there is no lateral interaction. Langmuir pictured monolayer formation to occur on the basis of a specific binding interaction between adsorbate molecules and distinct solid surface sites. This picture was originally founded on the results of experiments performed with hydrogen and other small molecules in the presence of heated metal filaments at very low pressures. In Langmuir 1918, this model was already broadly generalized to include cases where monolayer or multilayer formation occurs as well as cases ranging from highly regular surfaces to completely amorphous surfaces containing an abundance of different adsorption sites. The Langmuir theory of adsorption is useful for modeling and designing engineering processes, both qualitatively and quantitatively (Swenson & Stadie, 2019).The Langmuir model assumes that there is no interaction between the adsorbate molecules and the adsorption is localized in a monolayer form (Limousin et al., 2007). The Langmuir adsorption isotherm shows the equilibrium distribution of the ions between the solid and liquid phases. This model has been successfully applied to many real adsorption processes (Bilgiç & Çimen, 2019).The equation for Langmuir adsorption isotherm can be described as:-

$$\frac{C_e}{q_e} = \frac{1}{q_m} ce + \frac{1}{q_m K_L} \quad (3)$$

$$R_L = \frac{1}{1+K_L C_0} \quad (4)$$

Where, Ce = the equilibrium concentration of phosphate in the solution (mg/L), qe = the amount of phosphate adsorbed per gram of the adsorbent at equilibrium (mg/g), q_m = maximum monolayer coverage capacity (mg/g) or the maximum uptake corresponding to the site saturation, and K_L = Langmuir isotherm constant (L/mg) representing the ratio of adsorption and desorption rates. The separation factor R_L in eq (4) was used to evaluate the nature of the Langmuir isotherm. The R_L value tells the type of isotherm to be unfavorable (R_L > 1), linear (R_L=1), irreversible(R_L=0), 0<R_L<1 means that the reaction is well reversible, and favorable (R_L<1) (Y. Zhang et al., 2020; Y. Wang et al., 2021; Ajmal et al., 2018).

2.7.2. Freundlich adsorption isotherm model

The Freundlich isotherm model is an empirical relationship describing the adsorption of solutes from a liquid to a solid surface and assumes that different sites with several adsorption energies are involved. Freundlich isotherm model is the most important multi-site adsorption isotherm for heterogeneous surfaces (Deliyanni et al., 2007). It is one of the oldest models which are extensively used; it was developed by Freundlich in 1932**.** The Freundlich adsorption isotherm model is an empirical model expressed by the equation:

$$Logq_e = \frac{1}{n} LogC_e + LogK_F \quad (5)$$

Where qe is the amount of phosphate adsorbed per gram of the adsorbent at equilibrium (mg/g), Ce is the equilibrium concentration of phosphate in the solution (mg/L), KF is the Freundlich constant denoting adsorption capacity of the adsorbent (mg/g) or the distribution coefficient that represents the quantity of adsorbate adsorbed onto adsorbent for unit equilibrium concentration, *n* is the heterogeneity factor which is related to the intensity of adsorption (mg/L), and 1/*n* is an empirical constant related to the magnitude of the adsorption or surface heterogeneity. It also indicates the relative distribution of the energy and the heterogeneity of the adsorbate sites (Ayawei et al., 2017). A linear plot of Logqe versus LogCe provides the *K*F and *n* values. The Freundlich isotherm model is responsible for the heterogeneity of the adsorbent sites. For this study, Langmuir and Freundlich adsorption isotherm models were employed to describe the experimental results of phosphate ions adsorption.

2.8. Characterization of Nanoparticles and Composite

The characterization of nanomaterials is important for understanding their properties and applications. Characterization of noble metal nanoparticles for various applications is current areas of research. Strategies used for their fabrication and characterization are going to be improved day by day. Control over size and shape of nanoparticles is very important for their potential applications in various fields (Begum et al., 2018). The common methods used for the characterization of nanoparticles include, Ultraviolet visible (UV–Vis) spectroscopy, Scanning electron microscopy (SEM), Transmission electron microscopy (TEM), low energy electron diffraction (LEED), Extended X-ray absorption fine structure (EXAFS) used for the detection of surface topography, and Secondary ion mass spectroscopy (SIMS), Auger electron spectra (AES), Electron probe microanalysis (EPMA) (Mohammad Lou et al., 2016; Mourdikoudis et al., 2018). Each technique has its own advantages and disadvantages and it is hard to compare one technique to another because each technique has a specific purpose and used to get a specific information that cannot be obtained from the other one (K. Zhang et al., 2015).

2.8.1. Fourier transform infrared spectroscopy

Fourier Transform Infrared, the preferred method of infrared (IR) spectroscopy. In IR spectroscopy, IR radiation is passed through a sample. Some of the IR radiation is absorbed by the sample and some of it is passed through (transmitted). The resulting spectrum represents the molecular absorption and transmission, creating a molecular fingerprint of the sample. As two finger prints never match, similarly no two unique molecular structures produce the same IR spectrum (Yao et al., 2015). The functional groups of the materials were determined by using FTIR spectrometer. The infrared spectra is a fingerprint for identification by the comparison of the spectra from an ‘’unknown’’ with previously recorded reference spectra. The vibrational spectra of a molecule are considered to be an important physical property. It is a unique characteristic of the molecule. In the absence of a suitable reference database, it is possible to effect a basic interpretation of the spectrum from first principles, leading to characterization, and possibly even identification of an unknown sample (Coates, 2006). However, the application of FTIR in the characterization of functionalized nanoparticles could be difficult because it may not reveal the chemical bonds between the

nanoparticles and the functional molecules based on a database of known vibration frequencies. This is because the chemical bond between the functionalized molecules and the nano-material is usually novel, and thus, a strategy must be developed in order to provide evidence about the resonant vibration information between the grafted molecules and the nano-sized particles (Baudot et al., 2010). Biomolecules those are responsible for capping, reduction and stabilizer, are identify by using FT-IR (Ijaz et al., 2020).

2.8.2. X -ray diffraction

XRD is used for the determination of crystal structure, calculation of crystalline nanoparticles size and for confirmation of nanoparticles (Ijaz et al., 2020). The crystalline structure of nanoparticles can be calculated by using Debye Scherrer s equation (Muniz et al., 2016). The approximate average crystallite size of nanoparticles was determined by applying the Scherer formula:

$$D = \frac{0.9\lambda}{\beta\cos\theta} \quad (6)$$

Where D is the average particle size, λ wave length of the Cu-Kα irradiation, β the full width at half maximum intensity of the diffraction peak and θ is the diffraction angle. It provides information on structures, phases, preferred crystal orientations (texture), and other structural parameters, such as average grain size, crystallinity, strain, and crystal defects. XRD peaks are produced by constructive interference of a monochromatic beam of X-rays scattered at specific angles from each set of lattice planes in a sample. The peak intensities are determined by the atomic positions within the lattice planes. An online search of a standard database for X-ray powder diffraction patterns enables quick phase identification for a large variety of crystalline samples (Thurston et al., 2017).

2.8.3. Scanning electron microscope

SEM gives high resolution images of the surface of a sample. Output image formed by using SEM in which electron is used instead of light used to characterized shape, size, morphology and distribution of synthesized nanoparticles (Ijaz et al., 2020). The scanning electron microscope works as same principle as an optical microscope, but it measures the electrons scattered from the sample rather than photon. Because electrons can be accelerated by an

electric potential, the wavelength can be made shorter than the one of photons. This makes the SEM capable of magnifying images up to 200,000 times and measures the particle size and characterization, Conductive or sputter coated sample involved and the sensitivity down to 1nm (Kaur & Kaur, 2019).

2.8.4. Brunauer-emmett -teller (BET) characterization

Brunauer–Emmett–Teller (BET) theory aims to explain the physical adsorption of gas molecules on a solid surface and serves as the basis for an important analysis technique for the measurement of the specific surface area of materials. Specific surface area is a scale dependent property, with no single true value of specific surface area definable, and thus quantities of specific surface area determined through BET theory may depend on the adsorbate molecule utilized and its adsorption cross section. The fundamental element of BET theory is associated with the adsorption of a gas on the material's surface. This phenomenon is caused by van der Waals forces that are created by a film of the adsorbate, which consists of atoms, ions, or molecules on the surface of a substance that adsorbs these particles. The process of adsorption can be physical or chemical. While physical adsorption is related to van der Waals forces, chemical adsorption is a result of the chemical reaction between the solid and the adsorbate. The amount of the adsorbed gas on the adsorbent material can be correlated with its surface area (Ambroz et al., 2018). The BET gas adsorption method has become the most widely used characterization method for the determination of the surface area of finely-divided and porous materials. Because adsorption is a surface phenomenon, the degree of adsorption is proportional to the specific surface area. So the amount of adsorption accomplished per unit weight of solid adsorbent is greater if the solid is more finely divided and more porous. Substances like porous carbon, zeolite and silica gel are excellent adsorbents because they have a highly porous structure and hence have a large surface area (Crini et al., 2019).

2.8.5. Thermal gravimetric and differential thermal analysis

Thermogravimetric analysis or thermal gravimetric analysis (TGA) is a method of thermal analysis in which the mass of a sample is measured over time as the temperature changes. This measurement provides information about physical phenomena, such as phase transitions,

absorption, adsorption and desorption; as well as chemical phenomena including chemisorption, thermal decomposition, and solid-gas reactions (e.g., oxidation or reduction) (Mani et al., 2010). Differential Thermal Analysis (DTA) is a technique in which the difference in temperature between the sample and a reference material is monitored against time or temperature while the temperature of the sample, in a specified atmosphere, is programmed. In DTA, the material under study and an inert reference are made to undergo identical thermal cycles, (i.e., same cooling or heating programme) while recording any temperature difference between sample and reference. This differential temperature is then plotted against time, or against temperature (DTA curve, or thermogram). Changes in the sample, either exothermic or endothermic, can be detected relative to the inert reference. Thus, a DTA curve provides data on the transformations that have occurred, such as glass transitions, crystallization, melting and sublimation. The area under a DTA peak is the enthalpy change and is not affected by the heat capacity of the sample. Thermogravimetric analysis is conducted on an instrument referred to as a Thermogravimetric analyzer. A Thermogravimetric analyzer continuously measures mass while the temperature of a sample is changed over time. Mass, temperature, and time are considered base measurements in thermogravimetric analysis while many additional measures may be derived from these three base measurements. Thermogravimetric analysis is a widely used technique to obtain precise weight loss profile during thermal decomposition (Saadatkhah et al., 2020, Kumar et al., 2009).

2.9. Physicochemical Characteristics and Treatments of ASTU Wastewater

In the ASTU WWTP, biological treatment process with activated sludge technology with anaerobic sludge digestion and aerobic digestion was established. The wastewaters from the university environment come to the treatment plant through sewer network by gravity. The first stage in the WWTP is the screening for the removal of coarse material that if not removed, would damage the subsequent equipment and reduce process effectiveness. Generally, the screen is installed before grit removal units. The sand trap removes grit consisting of sand, gravel and other heavy solid materials that have subsiding velocities by 0.3m/s. A primary sedimentation is used to remove the undissolved organic material from the wastewater and therefore reduces the pollution load in the following biological process steps. The removed organic material, named as primary sludge, mainly contains of readily

biodegradable agents and is perfectly suited for further anaerobic digestion due to its high methane and other gases yield. The second stage in the wastewater treatment plant is the activated sludge process. This process is a common treatment method and has been implemented worldwide. The aeration tanks are dimensioned for the carbonaceous biochemical oxygen demands and chemical oxygen demands removal as well as nitrification and de-nitrification for the nitrogen removal. After some time, the mixture of biological solids is passed from the aeration tanks into the final sedimentation tanks, where some of the settled sludge is recycled to maintain the desired concentration of organisms in the reactor. The excess sludge is removed from the system and discharged to the imhoff tanks for the digestion and ultimately to sludge drying beds for the dewatering prior to the compositing. Even though the wastewater of the university is discharged by separate systems, groundwater and surface water will infiltrate into the sewer network.

2.9.1. Preliminary treatment

Preliminary treatment includes steps like screening which is the treatment process that used for removing coarse materials such as plastic, solids, rags, fats from the kitchen that significantly interfere the process and damage the plant equipment if not removed, and grit removal which is the essential process to remove substances such as sand, slit, glass, small stone as well as other large sized organic and inorganic substance that block operations and pumps of the reactors. The velocity of the channel must be kept at 0.3m/s. If the velocity below this value organic matters are settled in the channel as the sand. So this affects the process in the imhoff tank. If the velocity is above this value the inorganic matters are not settled instead it is flushed out of the channel and enters to the next step.

2.9.2. Primary treatment

The objective of primary treatment is the removal of settleable organic and inorganic solids by sedimentation, and the removal of materials that will float (scum) by skimming. Approximately 25 to 50% of the incoming biochemical oxygen demand (BOD5), 50 to 70% of the total suspended solids (TSS), 9% of total nitrogen, 11% of total phosphorous, and 65% of the oil and grease are removed during primary treatment. Some organic nitrogen, organic phosphorus, and heavy metals associated with solids are also removed during primary

sedimentation. It may be considered sufficient treatment if the wastewater is used to irrigate crops that are not consumed by humans or to irrigate orchards, vineyards, and some processed food crops. Settled solids (primary sludge) are normally removed from the bottom of tanks by sludge rakes that scrape the sludge to a central well from which it is pumped to sludge processing units. Scum is swept across the tank surface by water jets or mechanical means from which it is also pumped to sludge processing units. This process is anaerobic digestion process for 60 days at the temperature of 15^{o}C which have the volume of 2709m^{3}. The product of this treatment stage are sludge, gas and the over flow water which enters into aeration tank.

2.9.3. Secondary treatment

The objective of secondary treatment is the further treatment of the effluent from primary treatment to remove the residual organics and suspended solids. Aerobic biological treatment is performed in the presence of oxygen by aerobic microorganisms (principally bacteria) that metabolize the organic matter in the wastewater, thereby producing more microorganisms and inorganic end-products (principally CO_2, NH_3, and H_2O). Several aerobic biological processes are used for secondary treatment differing primarily in the manner in which oxygen is supplied to the microorganisms and in the rate at which organisms metabolize the organic matter. It uses biological processes to convert dissolved, suspended, and colloidal organic pollutants to more stable solids, which can be removed by settling.

Aerobic attached-growth treatment processes are those processes that utilize microorganisms that grow on a medium, such as stones and discs, to remove organic matter found in wastewater. They can also be used to achieve nitrification which is the conversion of ammonia to nitrate/nitrite. This treatment stage requires mixer and aerator. The function of aerator is giving oxygen to organic bacteria in order to grow and digest the organic pollutants in the waste water as well as it is used for making the activated sludge do not settled. It is operated for 1hour then the mixer opened. The mixer was used for mixing the wastes for the sake of activated sludge not settled and as well as for the purpose of nitrogen gas removal by de nitrification and formation of nitrate and nitrite by nitrification process. Mixer is also used for the balancing food to microorganism ratio. The aeration tank is designed as rectangular basins with circular flow, in which aerated areas act as carbon removal zones whereas

unaerated areas act as nitrogen removal zones. The aeration tank has a water depth of 3.0 m having the volume of 3201m^3. Aeration is realized through surface aerators. The oxygen supply to the aeration tanks is controlled by oxygen measurement devices. In the aeration tank, mixing is important for keeping the wastewater solids (Mixed liquor suspended solids, MLSS) in suspension. The aerators serve as both oxygen supplier and mixer. In addition to aerators, there are submerged mixers that mix the wastewater and keep MLLS in suspension in the aeration tank.

2.9.4. Final sedimentation

After the aeration tank, the over flow water is entered in to the final sedimentation (Dortmund tank). The final sedimentation tank serves as the separation of water and activated sludge. The effluent is discharged to the reservoir so called pollution pond where treated waters are stored. In order to stabilize the biological system with in the aeration tank, a certain amount of sludge is pumped back into it as return sludge. The excess sludge is pumped into the imhoff tank by submersible pumps. Return sludge pumps are installed in a pumping station, located between the final sedimentation tanks. Two submersible pumps (including one stand-by unit) are pumping the return sludge to the aeration tanks. Excess sludge pumps are installed in a pumping station, located among the final sedimentation tanks. The specific effluent characteristics of ASTU WWTP are mentioned in table 1.

Table 1: Effluent characteristics of ASTU WWTP

Parameter	Abbreviation	Values
Biological Oxygen Demand	BOD	20 -25mg/L
Chemical Oxygen Demand	COD	125 - 134mg/L
Dry Solids	DS	30 -50g/L
Total Kjeldahl Nitrogen	TKN	18 -25mg/L
Total Phosphorus	TP	5 -10mg/L
Total Dissolved Solid	TDS	40 – 75mg/L
Temperature	T	19 – 22 ^{0}C
pH	pH	4.5- 6

3. MATERIALS AND METHODS

3.1. Chemicals

In this study: Ferric chloride hexahydrate, $FeCl_3.6H_2O$ (Central Drug House, 99%) and Ferrous chloride tetrahydrate, $FeCl_2.4H_2O$ (Central Drug House, 99%) were used as precursors of iron oxide nanoparticles. Lanthanum (III) chloride tetrahydrate, $LaCL_3.4H_2O$ (Trust Chemical Laboratories, 98%) was used as precursor of $La(OH)_3$ NPs. Sucrose is used as precursor of porous carbon. Sodium hydroxide, NaOH (LOBA CHEMIE PVT.LTD, 98%), Hydrochloric acid, HCL (LOBA CHEMIE PVT.LTD, 35.4%), Sodium hydrogen carbonate, $NaHCO_3$ (CARELABMED CHEMICALS, 99%) and Tri sodium citrate, $Na_3C_6H_5O_7$ (Vision Chemicals, 98%) were used to adjust pH and for completion of the reaction (for precipitation process). Deionized water was used to prepare all solutions while Citric acid mono hydrate (CAMACHEM, 99%) was used to control the morphology of the adsorbent. Potassium dihydrogen phosphate, KH_2PO_4 (SAMIR TECH-CHEM, 97%) was used to prepare the standard solution. Ammonium molybdate solution, $(NH_4)_6Mo_7O_{24}\cdot 4H_2O$ (LOBA CHEMIE PVT.LTD, 99.3%), Potassium antimony tartrate solution, $K(SbO)C_4H_4O_6\cdot ½H_2O$ (LOBA CHEMIE PVT.LTD, 98%) and Ascorbic acid ($C_6H_8O_6$) solutions were used during UV-Vis spectrophotometer measurement. Ethanol (C_2H_5OH, 98%) was used further removal of impurities during synthesizing of nanoparticles and composite.Algae extract was used as reducing agent and surface modifier agent.

3.2. Methods

3.2.1. Collection and preparation of algae extract

Fresh green algae, *Kappaphycus alvarezii,* were collected from ASTU wastewater treatment plant. The collected fresh algae was first washed with tap water and then with Deionized water until no impurities remained. After that, the algae was dried under sunlight for 3 days and then cut into small pieces. In this study, 10 g of dried algae was weighed and put into a 150 mL beaker with deionized water and soaked for 24 hr. The mixture was then heated for 20 minutes at 60^oC while stirring occasionally and then allowed to cool at room temperature. After that the mixture was filtered by using the Whatman filter paper and then centrifuge for

15 minutes. The resulting extract was used as algae extract solution as shown in the Appendix (Figure II-1) (Pratiwi et al., 2019).

3.2.2. Synthesis of Fe_3O_4 nanoparticle using algae extract

Magnetite nanoparticles were developed through green synthesis method. First, 1.99 g of ferrous chloride tetra hydrate (M.mass = 199) and 5.41g of ferric chloride hexahydrate (M.mass = 270.5) was dissolved into a 150 mL conical flask with 50 mL deionized water to make a 2:1 M ratio and 10 mL of the algae extract was added into the same solution to obtain a brown colloidal solution under sonication for 10 minutes. Then, a freshly prepared 0.5 M NaOH solution was added drop-wise to the above mixture under continuous stirring at 500 rpm to adjust the pH to11. The solution was refluxed for one hour with continuous stirring at 70^oC to homogenize the solution and also for the completion of the reaction. After that, the synthesized Fe_3O_4 NPs were separated by using a permanent magnet and washed three times by using deionized water. The separated Fe_3O_4 NPs were dried in an oven at around 105^oC for 24 hours. The dried sample was stored in an airtight container for further analysis as shown in the Appendix (Figure II-2) (Yew et al., 2016).

3.2.3. Synthesis of lanthanum hydroxide nanoparticles using algae extract

Lanthanum hydroxide nanoparticles were synthesized using facile precipitation, following hydrothermal treatment methods. The synthesis procedure was as follows: 2.455 g of $LaCL_3 \cdot 4H_2O$ was dissolved in a 100 mL conical flask with 50 mL deionized water under constant stirring at 500 rpm for 30 minute. Then 10 mL of the algae extract was added to the dissolved lanthanum chloride solution. 0.5 M NaOH solution was added into the above mixture until the pH reached 10 under sonication for 10 minutes. Afterward, the mixture was stirred at 80^oC for 2 hr and then allowed to continue to react at room temperature for 24 hr to ensure that all the La ions completely transformed into $La(OH)_3$ nanocrystals which results a yellowish precipitates. The precipitate was washed three times with deionized water and then one time with ethanol to remove impurities and dried at 105^oC for 12 hr in a hot air oven. The dried sample was stored in an air-tight container for further characterization as shown in the Appendix (Figure II-3) (B. Wu et al., 2017).

3.2.4. Preparation of porous carbon

Porous carbon was prepared hydrothermal carbonization method with slight modifications as follows: approximately 2.5 g of sucrose ($C_{12}H_{22}O_{11}$) was thoroughly ground with 10 g of $NaHCO_3$ in a crucible and deionized water was added step by step to create a paste mixture. The paste mixture was then calcined at 400^oC for 3 hr in a crucible covered with another crucible in a furnace. The resulting blackish powders were mixed with 100 mL of 1M HCL solution in a 150 mL conical flask and stirred for 3 hr. The solid product was separated by filtration and washed three times with deionized water. The product was freeze- dried in a refrigerator at 4^oC for 12 hr, and the resulting material is referred to here as porous carbon (PC) as shown in the Appendix (Figure II-4) (Koilraj & Sasaki, 2017).

3.2.5. Synthesis of magnetic porous carbon (MPC)

Magnetic porous carbon composite was prepared by a hydrothermal process. In brief, Fe_3O_4 nanoparticles were developed on porous carbon as follows: 0.20 g porous carbon was suspended in 100 mL of deionized water under sonication for 30 minute in a 250 mL flask, and 1 g Fe_3O_4 nanoparticles were added in the porous carbon suspension. Under vigorous magnetic stirring at 60^oC in water bath for 0.5 hr, 0.5 M NaOH solution was added drop wise into the above suspension until its pH increased up to 11. Then 0.25 g of trisodium citrate was subsequently added for completion of the reaction and continuously stirred at 500 rpm for 1 hr at 80^oC. Finally, the product was washed with deionized water and absolute ethyl alcohol repeatedly and then dried at 80^oC overnight (Joshi et al., 2019).

3.2.6. Synthesis of $La(OH)_3$@Fe_3O_4@PC composites

$La(OH)_3$@Fe_3O_4@PC nanocomposites were prepared by a precipitation method. The precipitation method was adopted because of its simplicity, high efficiency, and low cost. $La(OH)_3$@Fe_3O_4@PC composite was prepared by adding 2 g of the previously synthesized magnetic porous carbon (MPC) into a 250 mL conical flask. 100 mL of the algae extract and 1g of the previously synthesized $La(OH)_3$ nanoparticles were added in to the same flask and stirred for 4 hr. Finally, 0.5 M NaOH solutions was added to the reaction mixture containing 0.5mmol citric acid to adjust the pH to 9 and refluxed at 80^oC for 1hr under constant magnetic stirring. Citric acid mono hydrate (99.8%) was used to control the morphology of the adsorbent. The precipitate was separated by applying external magnet. The separated

composite was washed three times with deionized water and ethyl alcohol respectively, and then dried at 105ºC overnight. The dried sample was stored in an air-tight container for further characterization as shown in the Appendix (Figure II-5) (Ahmed & Lo, 2020).

3.3. Characterization

In this thesis the synthesized nanoparticles; Fe_3O_4 NPs, $La(OH)_3$ NPs, porous carbon, magnetic porous carbon ,and $La(OH)_3@Fe_3O_4@PC$ composite were characterized by Fourier-transform infrared spectroscopy (FTIR), X-ray diffraction (XRD), Scanning electron microscope (SEM), Brunauer -Emmett- Teller (BET), and Thermal gravimetric analysis (TGA) methods.

3.3.1. Fourier-transform infrared spectroscopy (FTIR) characterization

The FTIR spectra of Fe_3O_4 NPs, $La(OH)_3$ NPs, porous carbon, magnetic porous carbon ,and $La(OH)_3@Fe_3O_4@PC$ composite were recorded by FT/IR6600 spectrometer in the range of 400 – 4000 cm^{-1} using the KBr disc method. Fourier Transfer Infrared Spectroscopy was used to determine the functional groups in the prepared nanoparticles and nanocomposites. It was used to identify the possible biomolecules/functional groups adhered to the surface of the nanoparticles and which might have acted as capping agents of the nanoparticles and the functional group of nanocomposites.

3.3.2. X-ray diffraction (XRD) characterization

The XRD was performed to investigate the crystalline or amorphous nature of the synthesized nanoparticles; Fe_3O_4 NPs, $La(OH)_3$ NPs, porous carbon, magnetic porous carbon ,and $La(OH)_3@Fe_3O_4@PC$ composite. The XRD of the nanoparticles and the composite adsorbents were tested at ASTU research laboratory of Material Science and Engineering Department using an X-ray diffractometer. The mass of approximately 0.5 g of the nanoparticles and the composite samples were measured for XRD characterization and filled in a sample holder. Then the sample was analyzed by using an X-ray diffractometer with Cu-Kα radiation source at λ= 1.5418 Å and operating at 40 kV and 30 mA. X-ray diffractograms of Fe_3O_4 NPs, $La(OH)_3$ NPs, porous carbon, magnetic porous carbon ,and $La(OH)_3@Fe_3O_4@PC$ composite were obtained for the 2θ angles scan range from 10˚ to 80˚ with a scan speed of 3˚/ min, and a counting time of 0.40 sec.

3.3.3. Scanning electron microscope (SEM) characterization

Adsorption of pollutants takes place on the surface of adsorbents. Thus, SEM is one of the most widely used surface identification methods. The porous carbon, magnetic porous carbon, and $La(OH)_3@Fe_3O_4@PC$ composite are characterized by a scanning electron microscope using a high-energy electron, and the out coming electrons are analyzed by applying a 10 kV electron acceleration voltage. These coming electrons give information about morphology, composition, the orientation of grains, and crystallography information of material. It provides information about the surface features and texture, shape, size, and arrangement of the particles on the sample surface (Grégorio Crini, Eric Lichtfouse, Lee Wilson, 2018; S. K. Sharma et al., 2018). For SEM, 10 mg sample of the nanoparticles and the composite were measured from the previously prepared sample and characterized by using scanning electron microscope.

3.3.4. Brunauer-emmett -teller (BET) characterization

Adsorption is a surface phenomenon. The degree of adsorption is proportional to the specific surface area. The adsorption capacity of adsorbents becomes higher if the solid is more finely-divided and more porous. The BET method can be used for the characterization of various types of microporous materials (Ambroz et al., 2018). The porous carbon, magnetic porous carbon, and $La(OH)_3@Fe_3O_4@PC$ composite are characterized by the Brunauer-Emmett-teller instrument. For BET characterization the empty samples cell were weighed using an electronic balance and 10.311 g of the samples were placed in the empty sample cells. Then the samples were degassed at temperature 150 ˚C for 60 minutes to remove impurity in the degas station of pore size and surface area analyzer according to the international union of pure and applied chemistry (IUPAC). After degassing, 0.2 g of the samples was placed in the analysis station in the range of 0.02 to 0.1 relative pressures and nitrogen gas concentration of 0.1 using Brunauer-Emmett-teller (BET).

3.3.5. Thermal gravimetric/ derivative thermogravimetric analysis

TGA records the weight loss as a function of temperature, while the derivative thermogravimetric (DTG) curve gives useful information about thermal decomposition stages involved during the overall heating process. The thermal degradation behavior of the $La(OH)_3@Fe_3O_4@PC$ adsorbent was observed with a Thermobalance detector, DTG-60H

(Model No: C30575100456TK, Korea). Approximately 15.463 mg of test sample was loaded into the crucible for analysis in the equipment. The experiment was carried out in an inert environment obtained by continuous flow of 50 mL/min of nitrogen gas that was used as non-oxidizing agent in order to determine the thermal stability of the $La(OH)_3@Fe_3O_4@PC$ composite. $La(OH)_3@Fe_3O_4@PC$ adsorbent was heated from 25°C to 900°C at a heating rate of 15°C/min.

3.4. Determination of Total Phosphorus by Ascorbic Acid Method

50 mL of 5 N Sulphuric acid, 5 mL Potassium antimony tartrate solution, 15 mL Ammonium molybdate solution and 30 mL Ascorbic acid solution were added in the order listed to prepare 100 mL of combined reagent. 8.0 mL of the combined reagent was added to 30 mL of sample solutions during every experimental activity for calorimetric determination of phosphate as antimony phosphate molybdate complex. Ammonium molybdate and antimony potassium tartrate react in an acid medium with dilute solutions of phosphorus to form an antimony-phospho-molybdate complex. This complex is reduced to an intensely blue-colored complex by ascorbic acid. The color is proportional to the phosphorus concentration. Only orthophosphate forms a blue color in this test. The absorbance of the solutions was measured automatically.

3.5. Batch Adsorption Experiments

During the adsorption process; dissolved species are transported into the porous adsorbent particle by diffusion and are then adsorbed onto the extensive inner surface of the adsorbent. The adsorption experiments were carried out in 250 mL Erlenmeyer flasks that contain 100 mL of phosphate solution. Stock solutions of phosphate were prepared by dissolving potassium dihydrogen phosphate (KH_2PO_4) in deionised water, and phosphate solutions within the concentration range of 5–300 mg/L were prepared. Briefly, 100 mL of phosphate solutions and 0.2 g of the composite were taken in a 250 mL stopper conical flask. The pH of phosphate solution was adjusted using dilute HCl and NaOH solutions by using pH meter. Equilibration for all adsorption experiments were done on a rotary shaker. The reaction mixture was shaken for 30 min at 200 rpm and 25°C and then separated by a magnet. The phosphate concentration of the supernatant was determined by the ascorbic acid method, measured at a wavelength of 750 nm using UV–vis spectrophotometer. Various adsorption experiments were performed using synthetic phosphate solutions to study the effect of the

following parameters on the adsorption of phosphate ions on the surface of the adsorbent. All experiments were performed at room temperature (Y. Zhang et al., 2020).

3.5.1. Effect of pH

The pH value plays an important role with respect to the adsorption of different ions on the adsorbents. The surface charge depends on the pH of the surrounding electrolyte. To study the influence of pH on the phosphate adsorption, experiments were carried out by adding 0.1 g of the adsorbent into 250 mL Erlenmeyer flask containing 100 mL of 100 mg/L phosphate solution and by varying pH of the solutions to 1, 3, 5, 7, 9, and 11 before adsorption experiments were carried out while keeping other parameters constant (agitation speed at 200 rpm, contact time at 1hr and initial phosphate concentration at 100 mg/L). The pH range (1 to 11) was selected based on the literatures (Fang et al., 2018; Ahmed & Lo, 2020; Lai et al., 2016). Each time the pH of the solutions were adjusted with dilute HCl or/and NaOH solution. The equilibrium phosphate concentration was measured after the solutions were agitated for 1 hr.

3.5.2. Effect of adsorbent dose

For determining the effect of adsorbent dose for phosphate adsorption, the amounts of phosphate ions adsorbed were determined by varying the dose as: 0.05, 0.1, 0.2, 0.4, 0.8 and 1 g in a 250 mL Erlenmeyer flask with initial phosphate concentration, agitation speed and contact time kept constant, and the pH value kept at the optimized value by adding 0.1 M HCl or 0.1 M NaOH solutions. The adsorbent dose (0.05, 0.1, 0.2, 0.4, 0.8 and 1 g) was selected and studied based on the literature (Y. Wang et al., 2021; Xie et al., 2014; Luo et al., 2021). The equilibrium phosphate concentration was measured after the solutions were agitated for 1 hr.

3.5.3. Effect of contact time

For determining the effect of contact time of phosphate adsorption, the amounts of phosphate ions adsorbed were determined by varying the contact time as 5, 15, 30, 60, 90, and 120 minutes in a 250 mL Erlenmeyer flask with pH and adsorbent dose being kept at the optimized values whereas, the agitation speed and initial phosphate concentration were kept constant. The contact time was selected based on efficiency of La-based adsorbents capacity

at these time intervals as different literatures reported (Abebe et al., 2018).The equilibrium phosphate concentration was measured after the solutions were agitated for 1 hr.

3.5.4. Effect of initial concentration

To study the effect of initial adsorbate concentration, the experiment was carried out using different initial phosphate concentrations (1, 50, 100, 150, 200, 250 and 300 mg/L). The initial concentration range was selected based on the literatures reported that La-based adsorbents capacity to adsorb phosphate concentration (Ismail et al., 2020). 100 mL of each of initial phosphate solution was added into a 250 mL Erlenmeyer flask that contains 0.2 g of the adsorbent. Each time the pH of the solution was maintained at the optimized value by adding 0.1 M HCl or 0.1 M NaOH solutions. The flasks were capped and shacked on rotator shaker at 200 rpm for 30 minutes to ensure approximate equilibrium. At the end of the adsorption period, each solution were filtered and then analysed for phosphate ions equilibrium concentration.

3.6. Adsorption Kinetics and Isotherm Study

Both kinetic and isotherm studies were carried out to differentiate the adsorption mechanism that occurred through the adsorption process. Effect of Phosphate ions adsorption kinetics was determined by varying the contact time as: 5, 15, 30, 60 and 120 minutes by keeping all parameters (pH, adsorbent dose, contact time, and initial phosphate concentration) at optimized value. It was evaluated by using 0.2 g of adsorbent and placed in several 250 mL Erlenmeyer flasks, each containing 100 mL of 50 mg/L phosphate solution. The pH of the solution was maintained at the optimized value. The flasks were stoppered and continuously shaken at a speed of 200 rpm. The sample solution was immediately filtered of and then analyzed for phosphate ions equilibrium concentration. The samples were collected at various time intervals. The equilibrium data were fitted to pseudo-first-order (eqn.1) and pseudo-second-order (eqn.2) model equations. Satisfactory conformity between experimental data and the model-predicted values were expressed by the correlation coefficient (R^2).

Phosphate ions adsorption isotherms were determined by varying the initial phosphate concentration from 1 to 300 mg/L while keeping all other parameters (pH, adsorbent dose, and contact time) at optimized conditions. In separate flasks, 100 mL of solutions containing different amounts of initial phosphate ions concentration were added. After the reaction

period, all samples were filtered and analysed for the corresponding phosphate ion concentration. The equilibrium data were fitted to the Langmuir (eq.3) and Freundlich (eq.5) isotherm models to determine the relationship between the adsorption capacity and the phosphorus concentration in solution at equilibrium. The amount of phosphate adsorbed onto the composite at the equilibrium (q_e) was calculated by the following equation:

$$Removal\ capacity(qe) = \frac{C_0 - C_e}{m}\ x\ V \quad (7)$$

Where C_0 and C_e are the initial and equilibrium phosphate concentrations in solution (mg P/L), respectively; V is the volume of solution (L) and m is the mass of adsorbent (g) (Ahmed & Lo, 2020).

3.7. Method of Phosphate Removal from ASTU WWTP Effluent

To study the phosphate removal efficiency of the synthesized $La(OH)_3@Fe_3O_4@PC$ composite, 50 mL sample from the effluent of the treatment plant were added into three each 250 mL Erlenmeyer flask that contains 0.2 g of the adsorbent. The pH of the solution were maintained at the optimized value by adding 0.1 M HCl or 0.1 M NaOH solutions. The flasks were capped and shacked on rotator shaker at 200 rpm at room temperature for 30 minutes to ensure approximate equilibrium. At the end of the adsorption period, each solution were filtered and then analysed for phosphate ions equilibrium concentration by UV-vis spectrophotometry.

3.8. Regeneration of Synthesized $La(OH)_3@Fe_3O_4@PC$ Composite

Desorption of adsorbed phosphate with a proper method would be important when one considers to reuse the adsorbent for phosphate removal after it was saturated. The desorption processes are significant for the regeneration of adsorbents for reuse in other adsorption processes. The reusability of the used adsorbent $La(OH)_3@Fe_3O_4@PC$ adsorbent was investigated by performing six successive adsorption-desorption cycles of phosphate ions on the $La(OH)_3@Fe_3O_4@PC$ adsorbent by using 0.1 M NaOH desorption solution. The adsorption of phosphate by 0.2 g of $La(OH)_3@Fe_3O_4@PC$ adsorbent at pH of 5, initial phosphate concentration of 50 mg/L, 200 rpm agitation speed, and contact time of 30 minute at 25 °C was done, followed by desorption of adsorbed phosphate with 0.1 M NaOH solution after each cycle. After 30 minutes of adsorption of 50 mg/L phosphate solution by the nanoadsorbents, phosphate desorption experiments were conducted by reacting the recovered

adsorbents in 50 mL of 0.1M NaOH desorption solution on a shaker for 60 minutes at room temperature. The supernatant sample was withdrawn for analyzing the phosphate desorption efficiency. Then magnetic adsorbent was separated, washed and dried at 60^0c for 2 hr.

The reusability of the regenerated adsorbent was calculated for the above adsorption-desorption experiments six times. In order to assess the possibility of recycling the adsorbent, the percentage of phosphate desorbed to adsorb was calculated. Desorption efficiency was calculated by the equation:

$$Desorption\ efficiency(\%) = \frac{C_{desorbed}}{C_{adsorbed}}\ x\ 100 \qquad (8)$$

Where $C_{desorbed}$ is the amount of the phosphate ion that was removed from the loaded powder after desorption study, $C_{adsorbed}$ is $C_0 - Ce$ for each recovery process, C_0 is the initial phosphate concentration, and Ce is the equilibrium phosphate concentration in mg/L(Abebe et al., 2018, Ahmed et al., 2019, Y. Chen et al., 2020).

4. RESULTS AND DISCUSSIONS

4.1. Characterization

4.1.1. X-ray diffraction (XRD) analysis results

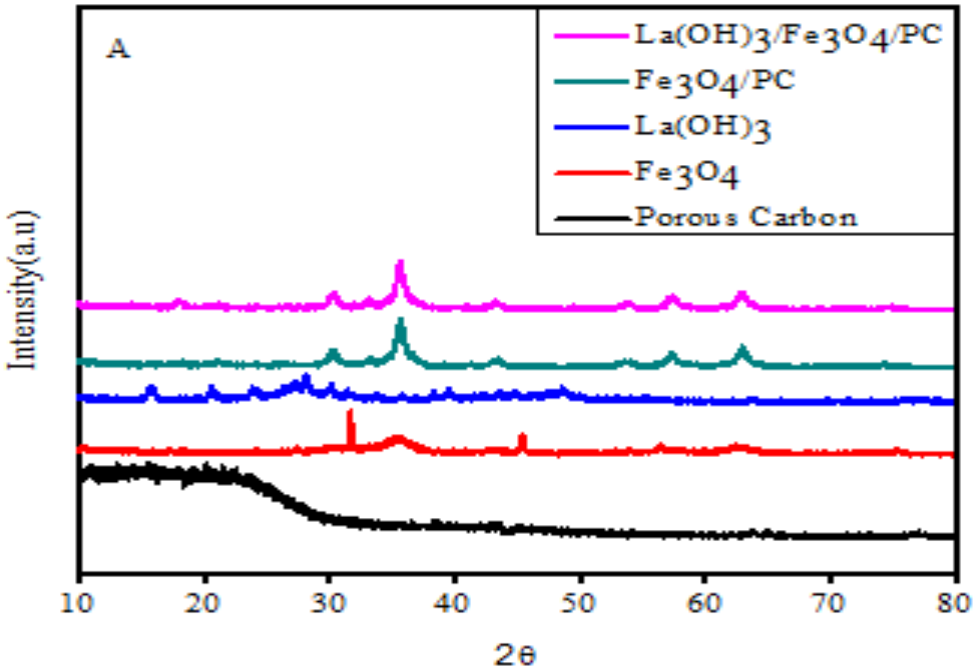

Figure 4: XRD pattern of PC, Fe_3O_4NPs, $La(OH)_3$NPs, Fe_3O_4/PC, and $La(OH)_3$@Fe_3O_4@PC**.**

Figure 4 shows the XRD patterns of porous carbon, Fe_3O_4 NPS, $La(OH)_3$ NPS, and $La(OH)_3$@Fe_3O_4@PC composite. The XRD patterns for the nanomaterials were primarily amorphous and only few crystalline phases were detected. The XRD patterns of the prepared PC showed a broad reflection at approximately 24° in 2θ which is suggestive of an amorphous phase (Koilraj & Sasaki, 2017). The crystal structure of the green synthesized magnetite nanoparticles was evidenced by the diffraction peaks, with the strong ones appearing at 2θ values of 32, 35, 43, 57, 63, and 75 respectively. These are the characteristic peaks of the pure phase magnetite Fe_3O_4 nanoparticles at 220, 311, 411, 511, 440, and 420 reflections respectively. These results corresponds to the standard pattern for cubic magnetite (JCPDS No.19-0629) (Ahmed & Lo, 2020; Daneshvar Tarigh & Shemirani, 2013). The diffraction peaks revealed that the obtained products were pure spinel phase magnetite Fe_3O_4 nanoparticles displaying some reflection peaks in the 2θ region of 10–80° (Yuvakkumar &

Hong, 2014). Similar findings was reported for magnetite nanoparticles with intensity of the diffraction peaks at 2θ of 35°, 57° and 63° corresponding to the 311,511 and 440 planes of the magnetite Fe_3O_4 structure (JCPDS 75-1609) (Yang et al., 2015;Viju Kumar & Prem, 2018). By using Scherer formula eq (6), the calculated average crystallite size of the synthesized magnetite NPs was found to be 2.85nm.

Table 2: The peak positions and crystalline sizes of the synthesized Fe_3O_4 NPs.

Peak position(2θ)	FWHM	size of the nanoparticle (nm)	Average size (nm)	hkl
35.34	2.99853	2.780479751	2.852316524	311
57	3.39241	2.664648093		220
62.70	2.98916	3.111821727		440

Characteristic peaks at 2θ = 15.74, 27.42, 38.86, 48.28, 55.14, and 63.56 due to reflections from 100, 110, 101, 210, 302, and 211 planes of hexagonal $La(OH)_3$ were observed. These six peaks of low intensity correspond to the hexagonal phase of lanthanum hydroxide (JCPDS No. 36-1481). All peaks can be perfectly indexed as the pure hexagonal phase (P63/m (176), Joint Committee on Powder Diffraction Standards (JCPDS) file number 36-1481) of $La(OH)_3$, with lattice constants a = 6.529 Å and c = 3.859 Å. Similar results have been reported recently(Fang et al., 2018) (Ahmed & Lo, 2020). By using Scherer formula eq (6), the calculated average crystallite size of the synthesized lanthanum hydroxide NPs was found to be 10.34 nm.

Table 3: The peak position and crystalline size value of the synthesized $La(OH)_3$ NPs**.**

Peak position(2θ)	FWHM	size of the nanoparticle (nm)	Average size (nm)	hkl
15.74	0.55626	14.41797601	10.34070974	100
27.42	0.49855	16.195864		110
38.86	1.06698	7.612942941		101
48.28	1.936	5.684196205		210
55.14	0.15291	7.792569516		302

Diffraction peaks at 2θ = 18, 29, 32, 35, 43, 55, 57, 63 and 74 were mainly observed in the synthesized composite which also exist in the synthesized Fe_3O_4 and $La(OH)_3$ nanoparticles. The presence of both Fe_3O_4 and $La(OH)_3$ diffraction peaks in the nanocomposite indicates a crystalline nature of $La(OH)_3@Fe_3O_4@PC$ composite (Mazloumi et al., 2009; Ahmed & Lo, 2020; Ahmed et al., 2021). This indicates that magnetite and lanthanum hydroxide nanoparticles are loaded on the surface of the porous carbon since the composite is less crystalline than the magnetite nanoparticles (Lai et al., 2016). By using Scherer formula eq (6), the calculated average crystallite size of the synthesized $La(OH)_3@Fe_3O_4@PC$ composite was found to be 10.04 nm.

Table 4: The peak position and crystalline size of the synthesized nanocomposites.

Peak position(2θ)	FWHM	size of the nanoparticle (nm)	Average size (nm)
18.04	0.63952	12.57786167	10.044953
21.16	0.71126	11.362423	
32.31	0.79478	10.35565309	
35.67	1.03695	8.047986837	
43.32	0.69686	12.26622139	
54.80	1.02207	8.715829491	
57.37	1.01269	8.942227759	
62.99	1.15146	8.091420789	

4.1.2. Fourier-transform infrared spectroscopy (FT-IR) analysis results

FTIR was used to identify the possible biomolecules/functional groups adhered to the surface of the nanoparticles and which might have acted as capping agents of the nanoparticles and the functional group of nanocomposites. The FTIR analysis was performed in order to establish the changes in the functional groups of the nanoparticles and the composite (Ismail et al., 2020; Viju Kumar & Prem, 2018). Fourier Transfer Infrared Spectroscopy (model FT/IR6600, JAPAN) was used to determine the functional groups in the prepared nanoparticles and nanocomposites.

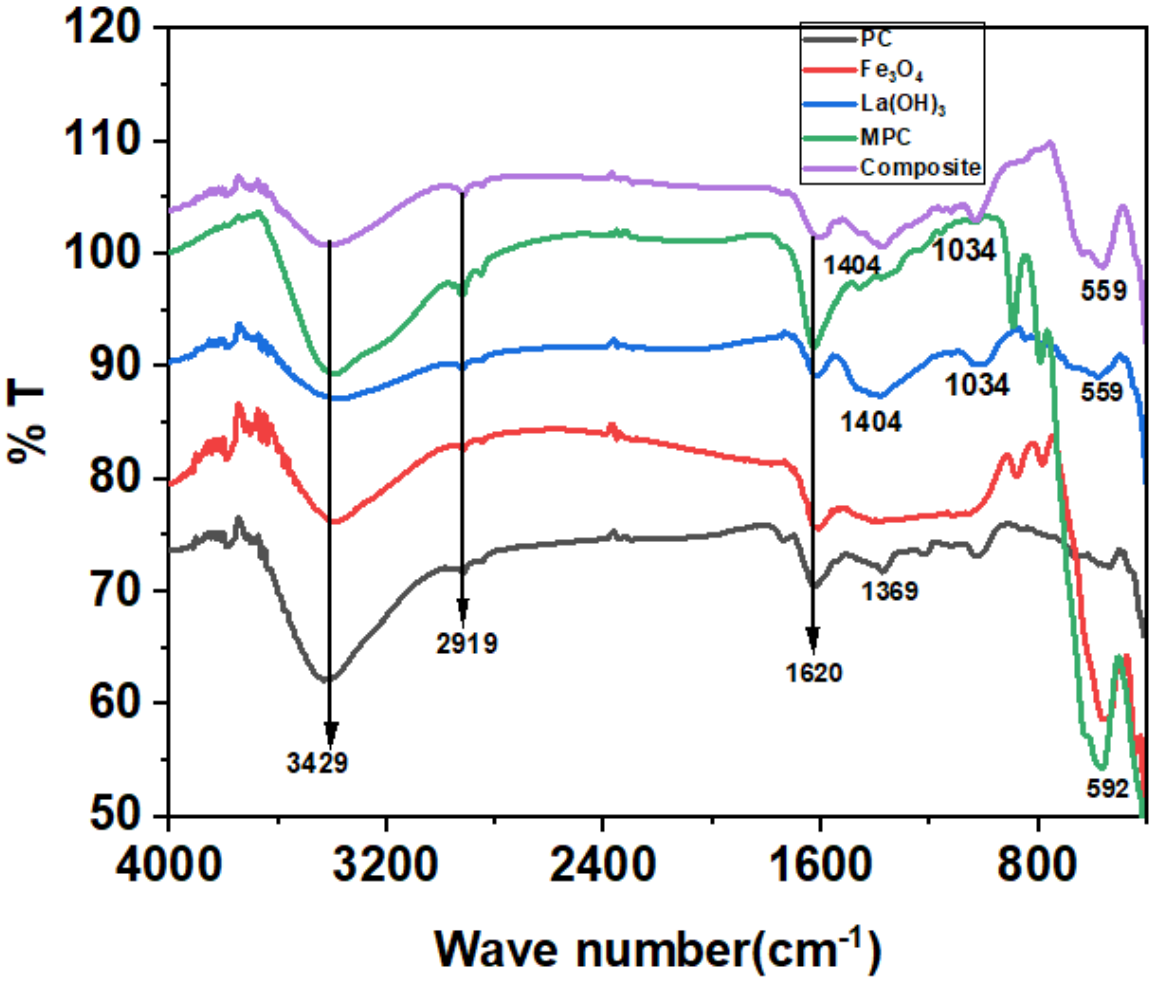

Figure 5: FTIR spectra for the PC, Fe_3O_4, $La(OH)_3$, MPC and $La(OH)_3@Fe_3O_4@PC$.

FTIR spectra of the PC, Fe_3O_4, $La(OH)_3$, MPC and $La(OH)_3@Fe_3O_4@PC$ PC are provided in Figure 5. All of the materials showed a broad band at 3429 cm^{-1} that corresponds to the O-H stretching vibration mode of surface-adsorbed water molecules. The bands at 2919 and 2855 cm^{-1} correspond to the aliphatic –C-H stretching vibration mode. A small band observed at 1620 cm^{-1} is assigned to the stretching aromatic C=C vibration mode and band at 1369 cm^{-1} corresponds to asymmetric –C-H stretching which may be caused by the presence of ester, ether, carbonyl, or aromatic functional group on the surface of nanomaterials (B. Chen et al., 2011). A characteristic peak at around 592 cm^{-1} corresponds to the Fe-O stretching band of magnetite (Fe_3O_4). This small sharp peak confirms the presence of Fe_3O_4 NPs. Characteristic peaks as the peaks lying in the region between 400 and 600 cm^{-1} were corresponding to Fe_3O_4 (B. Chen et al., 2011; Viju Kumar & Prem, 2018;Yuvakkumar & Hong, 2014). The distinct

band observed at 559 cm^{-1} is characteristic of the La-OH bond vibrations in $La(OH)_3$ (Song et al., 2020; Koilraj & Sasaki, 2017; Fu et al., 2018). The peak at 1404 cm^{-1} was related to the stretching vibration of the carboxylate group, C=O. The above observed FTIR spectra confirm the presence of organic impurities in the sample and some from the algae extract during the preparation of the $La(OH)_3$ nanoparticles (mousavi et al, 2015). The peak at about 1034 cm^{-1} can be attributed to the carbonate group, which originate from the reaction of $La(OH)_3$ with CO_2 from air during the analysis (Aghazadeh et al., 2011). The FTIR results clearly indicate that the Fe_3O_4 and $La(OH)_3$ nanoparticles have been loaded into the composite (X. Liu et al., 2019).

4.1.3. Scanning electron microscope (SEM) analysis results

Scanning electron microscopy is used to obtain information on surface morphology and provides information about surface area available for adsorption. The size and the morphology of the synthesized nanoparticles were confirmed by employing this technique (Batool et al., 2018). Surface morphology of the porous carbon, magnetic porous carbon and the magnetic composite were examined by using scanning electron microscopy (SEM) to investigate the shape, size, and porosity of the materials asshown in Figure 6. Scanning Electron Microscopy (JCM-6000PLUS Bench Top SEM JEOL, Japan) was used to determine the morphology of the samples. From SEM results it is clear that the nanoparticles synthesized possess different structures. The green method adopted synthesized particles (Figure 6 B and C) are seems to be more sticky, and have an aggregated form.

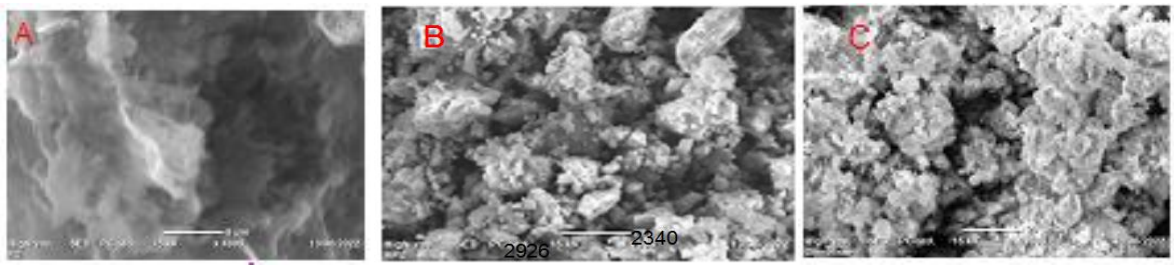

Figure 6: SEM images of PC (A), MPC (B) and La $(OH)_3$@Fe_3O_4@PC composite (C).

SEM image showed that the prepared carbon is highly porous (Figure 6A). The pores are likely created by the expulsion of CO_2 during the thermal treatment of the starch during carbonization process at 400^0c (Koilraj & Sasaki, 2017). Figure 6B shows the SEM image of

Fe_3O_4/PC(MPC), from which it can be seen that Fe_3O_4 nanoparticles are sufficiently loaded on the porous carbon , and aggregation occurred due to the magnetic properties of Fe_3O_4, leading to the uneven distribution of Fe_3O_4 on the surface of the porous carbon (Y. Wang et al., 2021). In addition, the SEM image (Figure 6C) showed that $La(OH)_3$ covered the surface of MPC in an irregular shape during the synthesis process. $La(OH)_3$@Fe_3O_4@PC composite exhibited agglomeration of particles with a rough surface, which was attributed to the further loading of $La(OH)_3$ (Figure 6C) (Y. Chen et al., 2020). The SEM image in Figure 6C showed that the $La(OH)_3$@Fe_3O_4@PC composite has a more compact structure than the porous carbon as well as the magnetic porous carbon. There is an aggregation of particles that cannot be observed in SEM micrographs (Ahmed et al., 2021). A close investigation of the surface structures which was obtained by the high-magnification SEM (Figure 6), shows that the whole rough surface is stacked by multilayer nanoparticles aligned irregularly in different dimensions (Xie et al., 2014; Aghazadeh et al., 2011; Zheng et al., 2021).

4.1.4. Brunauer-emmett-teller (BET) analysis results

The BET analysis was done by using a Horriba surface area analyzer with model number SA-9600. The BET specific surface area of the synthesized PC was found to be 374.1m^2/g. After being coated with a layer of magnetite nanoparticles, the surface area decreased to 151.450m^2/g. Functionalization of the surface of magnetic porous carbon by lanthanum hydroxide nanoparticles caused further decrease in surface area to 103.264m^2/g. The decrease of the BET surface area may be due to the formation of aggregated nanocomposites and the increase in the particle size of the nanocomposites. The BET isotherm type is type I, C =190.6(C> 150), micro porous material with pore diameters less than 2 nm with monolayer volume of 0.009. Pseudo-Langmuir isotherm with monolayer adsorption process and micropore filling occurs. Similar results were also observed in other La-based adsorbents (B. Wu et al., 2017, Lai et al., 2016). These changes in structure characteristics may be attributed to the incorporation of lanthanum hydroxide inside the mesoporous or aggregation onto the surface of magnetic porous carbon. However, the obtained results suggested that lanthanum can be successfully incorporated into the mesoporous structure of magnetic porous carbon (He et al., 2017; Y. Zhang et al., 2020).

4.1.5. Derivative thermogravimetric and thermogravimetric analysis results

From the derivative thermogravimetric (DTG) graph as shown in Figure7, the maximum thermal degradation temperature of the $La(OH)_3@Fe_3O_4@PC$ adsorbent was around 408^oC. Thermal decomposition of $La(OH)_3@Fe_3O_4@PC$ adsorbent occurred in three stages. First stage of the decomposition occurred at a temperature of 71.10^oC (-6.28uV) which corresponded to an initial weight loss of around 0.5% or around 0.0773mg. This may be due to the moisture evaporation or low molecular weight volatile compounds (Saadatkhah et al., 2020, Ramos Filho et al., 2005). Second stage of the decomposition contributed to a major weight loss of about 2.302mg at a temperature of 407.75^oC (47.70uV). This weight loss is around 14.887% of the total initial weight. This major weight loss may be due to the decomposition of the adsorbent in to other forms by releasing carbon dioxide or carbon monoxide gases. This result implies that $La(OH)_3@Fe_3O_4@PC$ adsorbents have low thermal stability. In the final stage, from temperature range of 500-900^oC, the weight loss curve was almost flat. There is no decomposition of $La(OH)_3@Fe_3O_4@PC$ adsorbent at this temperature range. This may be because the adsorbent is converted in to non-volatile inorganic ashes (Saadatkhah et al., 2020). Thus the suitable working temperature of the $La(OH)_3@Fe_3O_4@PC$ adsorbent should be below 300^oC since the composite is more stable at this temperature range. For the DTA curve obtained according to Fig. 7 in the low-temperature range of ΔT=50^oC–200^oC, an endothermic effect was found for the nanocomposite under study. The maximum value of exothermic peak temperature, Tmax = 408^oC is observed for the $La(OH)_3@Fe_3O_4@PC$ adsorbent. It should be noted that the shift of exothermic peak to the high-temperature region indicates not only improved cohesive properties, but also the thermal stability under the influence of a thermal field. On the basis of the performed thermogravimetric and differential thermal analyses, it can be stated that the $La(OH)_3@Fe_3O_4@PC$ adsorbent has the high heat resistance characteristics (Buketov et al., 2014).

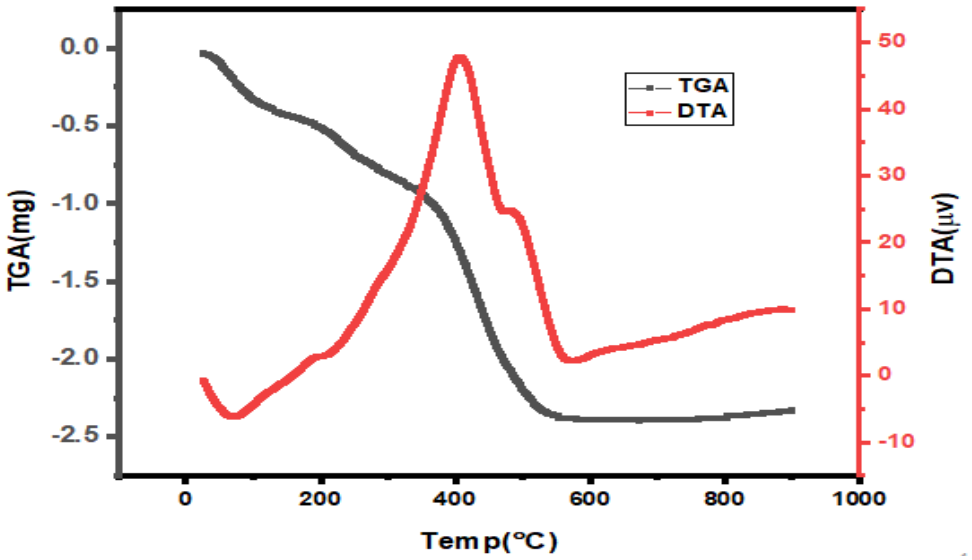

Figure 7: TGA/DTG plots of $La(OH)_3@Fe_3O_4@PC$ adsorbent(initial heating rate is 15^0C/min).

4.2. Optimization for Removal of Phosphate from Wastewater

4.2.1. Effect of pH

The effects of pH on the phosphate adsorption by $La(OH)_3@Fe_3O_4@PC$ adsorbent was studied over a wide pH range from 1up to 11, at a phosphate concentration of 100 mg/L. According to the results shown in Figure 8, it is obvious that the adsorption of phosphate ion on the $La(OH)_3@Fe_3O_4@PC$ adsorbent was strongly pH-dependent. It shows that the phosphate removal extents of the adsorbent gradually increase when pH increases from 3(99.838%) to 5(99.934%), while the removal extents starts to decrease at pH 7(94.416%). The phosphate removal extent of the $La(OH)_3@Fe_3O_4@PC$ adsorbent decreases at a higher pH value and reaches to 85.053% removal extent at a pH of 11. The decrease in the phosphate adsorption efficiency at pH < 5 may be due to the formation of phosphoric acid from phosphate when the environment becomes highly acidic (Deliyanni et al., 2007) as well as dissolution of La from $La(OH)_3@Fe_3O_4@PC$ adsorbent, which was supported by La leaching test mentioned in other studies (Fang et al., 2018; He et al., 2017). It is known that phosphoric acid can dissociate to form different ionic species of $H_2PO_4^-$, HPO_4^{2-}, and PO_4^{3-}, depending on the pH of solution as expressed by the following reaction:

$H_3PO_4 \leftrightarrow H_2PO_4^- + H^+$, $pKa_1 = 2.15$

$H_2PO_4^- \leftrightarrow HPO_4^{2-} + H^+$, $pKa_2 = 7.20$

$HPO_4^{2-} \leftrightarrow PO_4^{3-} + H^+$, $pKa_3 = 12.33$ (W. Y. Huang et al., 2014). When the pH value is between 2.15 and 7.20, the main species in the solution is monovalent $H_2PO_4^-$. Meanwhile, lanthanum is most likely present in its protonated form of $La(OH)_2^+$. The high adsorption capacity (Figure 8), observed in the pH range of 3–5, indicates that the lanthanum deposited on the magnetic porous carbon surface works as an active site, providing a great affinity to the monovalent phosphate species $H_2PO_4^-$. This is related to the surface charge on the $La(OH)_3@Fe_3O_4@PC$ adsorbent. According to several studies, La-based adsorbents have positive surface charge at a pH below 7 (Ahmed & Lo, 2020; B. Wu et al., 2017). The positive surface charge of the $La(OH)_3@Fe_3O_4@PC$ adsorbent at low pH favours electrostatic interaction and leads to an enhanced removal capacity (Makita et al., 2020, Ahmed & Lo, 2020). The efficiency of the $La(OH)_3@Fe_3O_4@PC$ adsorbent to adsorb phosphate decreases at relatively high alkaline conditions because the fraction of bivalent HPO_4^{2-} species gradually increases and predominates in water in addition to the presence of monovalent $H_2PO_4^-$ species (Fang et al., 2018). The adsorbent surface could have lower affinity for divalent HPO_4^{2-} compared to monovalent $H_2PO_4^-$. Previous studies also suggested that lanthanum ions have greater affinity for monovalent $H_2PO_4^-$ due to the hydroxylation of lanthanum ions (L. Zhang et al., 2011). Such behavior has also been observed during phosphate adsorption onto other La-based adsorbents (Fang et al., 2018; Ahmed & Lo, 2020; Lai et al., 2016). The adsorption of phosphate by the composites was believed to have occurred through surface complexation/precipitation with $La(OH)_3$ via ligand exchange, which was supported by an increase in the pH of the solution. Precipitation with surface-adsorbed La^{3+} ions also likely occurs due to the low K_{SP} of LaPO4 ($K_{SP} = 3.7 \times 10^{-23}$).

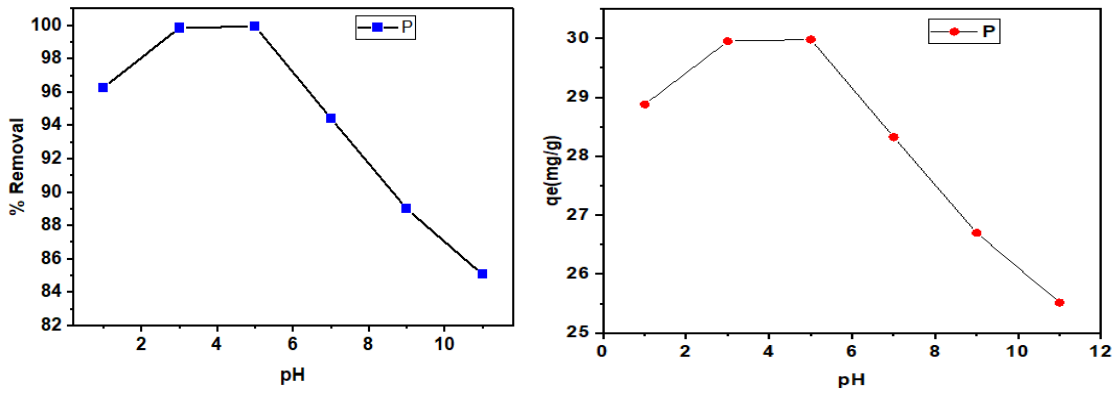

Figure 8: Effect of pH on the removal of phosphate [Co = 100 mg/L, dose = 0.1 g, agitation speed = 200 rpm and contact time = 1 hr].

4.2.2. Effect of dosage

The phosphate removal rate and adsorption capacity at different adsorbent dosing levels were investigated to determine the appropriate dose level of $La(OH)_3@Fe_3O_4@PC$ adsorbent. The influence of adsorbent dosage on phosphate removal was studied by varying the $La(OH)_3@Fe_3O_4@PC$ adsorbent dose from 0.05 to 1 g/L and by keeping other variables constant like pH at 5 , contact time at 60 min, 100 mg/L initial phosphate concentration, agitation speed at 200 rpm and at room temperature. The results in Figure 9 shows that the percent removal of phosphate by the $La(OH)_3@Fe_3O_4@PC$ adsorbent rapidly increase from 94.051% to 99.928% as the dose changes from 0.1 to 0.2 g. This increase in percent removal with an increase in $La(OH)_3@Fe_3O_4@PC$ adsorbent dose may be due to the availability of more active sites in the adsorbent surface (Abebe et al., 2018). Increased adsorbent dosage implied a greater surface area and a greater number of binding sites available for the constant amount of phosphate. It is also observed that a further increase of adsorbent dose from 0.2 to 1 g, the percent adsorption increases less significantly. This result is in an agreement with the findings of phosphate adsorption to other lanthanum-based sorbents (Y. Wang et al., 2021; Xie et al., 2014; Luo et al., 2021). Thus, the adsorbent dose was maintained at 0.2 g in all the subsequent experiments, which was considered to be sufficient for the removal of phosphate. Therefore, as shown in Figure 9, the percent removal (%) of phosphate initially increased sharply with increasing $La(OH)_3@Fe_3O_4@PC$ adsorbent dose, reaching nearly 100%. It is worth noting that by adopting an appropriate $La(OH)_3@Fe_3O_4@PC$ adsorbent dosage, near

complete removal of phosphate from aqueous solutions could be achieved as it can be seen in the appendix(I).

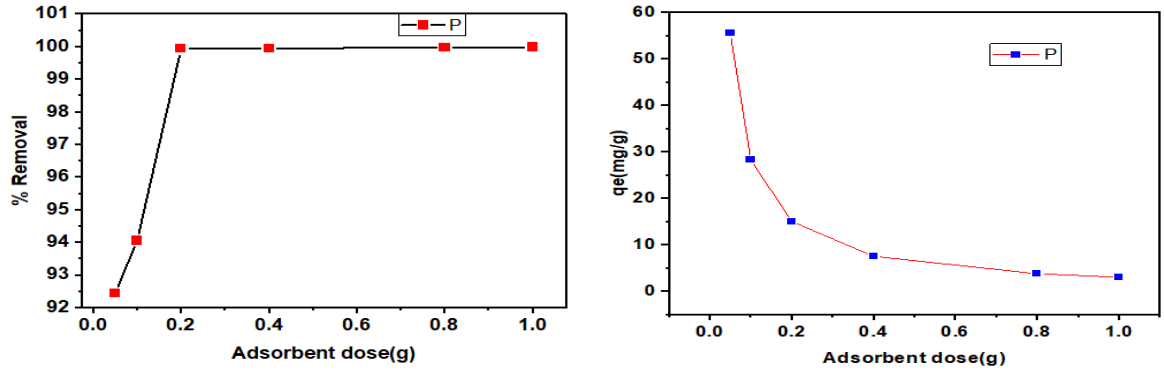

Figure 9: Effect of adsorbent dose on the removal of phosphate [Co = 100 mg/L, agitation speed = 200 rpm, pH = 5, and contact time = 1 hr].

4.2.3. Effect of contact time

The effect of contact time between the adsorbate ions and $La(OH)_3@Fe_3O_4@PC$ adsorbent on the adsorption efficiency of phosphate were investigated by experimenting with 5, 15, 30, 60, 90, and 120 minutes of contact time at 200 rpm agitation speed at room temperature. Other parameters were kept constant like pH at 5, initial phosphate concentrations at 100 mg/L, and dose at 0.2 g. From the results presented in Figure 10, the rate of percent removal is higher at the beginning because of the large number of vacant surface sites available for adsorption. The maximum adsorption of phosphate (99.936%) on $La(OH)_3@Fe_3O_4@PC$ adsorbent was obtained at contact times of 30 minute due to the strong electrostatic attraction between the positively charged adsorbent and the negatively charged phosphate ions. After this equilibrium contact time, a slight decrease in the adsorption capacity of the $La(OH)_3@Fe_3O_4@PC$ adsorbent was observed. This may be due to the competition for the adsorption sites on the adsorbent by other ions like hydroxide ions from the solution (Luo et al., 2021).

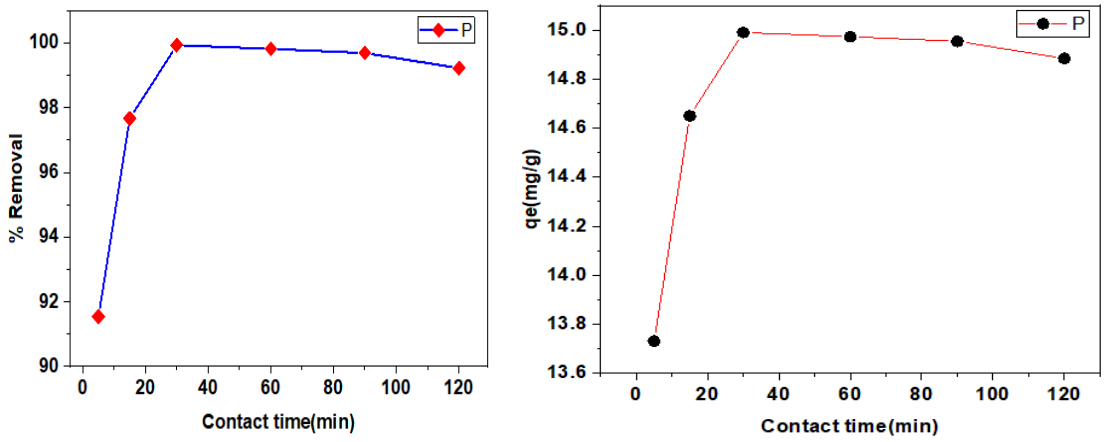

Figure 10: Effect of contact time optimization on the removal of phosphate [Co = 100 mg/L, adsorbent dose = 0.2 g, agitation speed = 200 rpm and pH = 5].

4.2.4. Effect of initial concentration

The effect of the initial concentration of phosphate ions in the solution towards adsorption efficiency was studied. Initial concentration of phosphate was studied by varying the concentration and keeping other variables constant. In this study, the initial concentration of 1, 50, 100, 150, 200, 250, and 300 mg/L at pH 5, adsorbent dose of 0.2 g, contact time 30 min, agitation speed 200 rpm were used. As shown in Figure 11, the percentage removal decreases with increasing initial concentration. This is because the adsorbent has a fixed capacity and can adsorb only a maximum specified amount. Thus additional adsorbate concentrations do not get adsorbed. Hence, the percentage removal decreases starting from the saturation point. From Figure 11, it can be seen that adsorption efficiency initially increases with increasing phosphate concentration from 99.60% at concentration of 1mg/L and an optimum maximum value reached at concentrations of 50 mg/L with percent removal of 99.87% and it becomes decrease with an increase in initial concentration. This is due to the lack of active sites of the $La(OH)_3@Fe_3O_4@PC$ adsorbent (Ismail et al., 2020). The increase in the initial concentration up to a certain point shows an increasing removal of phosphate ions as much as available active sites occurs. However, an additional increase in the adsorbate ions results in the reduction of removal efficiency. The removal efficiency of the phosphate ion decreased from 99.87% at 50 mg/L to 96.50 % at 150 mg/L. This can be explained by the fact that in case of low concentrations, the ratio of the initial number of moles of solutes to the

available surface area of adsorbent is large and subsequently the fractional adsorption becomes independent of initial concentration and consequently higher adsorption yields were obtained. However, at higher concentrations, most of the adsorption sites could be occupied by ions and the available sites of adsorption would become fewer, hence the percentage removal of phosphate ions which depends up on the initial concentration could decrease (Abebe et al., 2017).

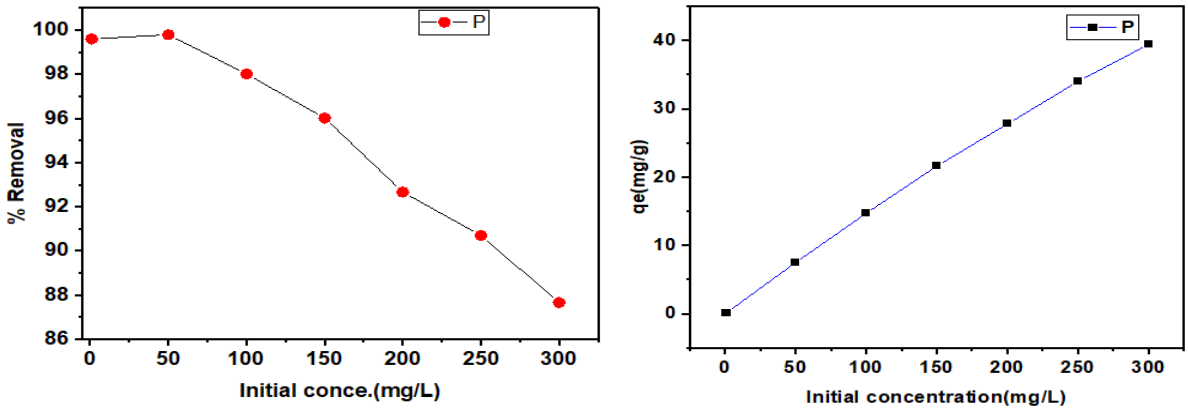

Figure 11: Effect of initial concentration of phosphate on the removal of phosphate

[Adsorbent dose = 0.2 g, contact time = 0.5 hr**,** pH = 5 and agitation speed = 200 rpm].

4.3. Kinetics Study

The kinetics of phosphate ions adsorption onto $La(OH)_3$@Fe_3O_4@PC adsorbent was analyzed by using pseudo-first-order and pseudo-second-order kinetic models. The kinetics study were done using pH 5 , initial phosphate concentration of 50 mg/L, adsorbent dosage 0.2 g, agitation speed 200 rpm at room temperature. By using the correlation coefficient significance, the conformity between experimental data and the model-predicted values were expressed. The phosphate uptake was very rapid in the first 15 minute and adsorption equilibrium was achieved with in 30 minute similar to other La-based adsorbent studies (B. Wu et al., 2017, Song et al., 2020).

4.3.1. Pseudo-first order kinetic model

To determine whether the adsorption process fits with the pseudo-first-order model or not, the experimental data using contact time ranging from 5 - 120 min and pH 5, initial phosphate concentrations 50 mg/L, adsorbent dosage of 0.2 g at room temperature, and 200 rpm

agitation speed were introduced to Equation 1. From the slopes and intercepts of pseudo-first order model [Log (qe-qt) versus t] (Figure 12), the first order rate constant, k_1 and equilibrium adsorption density, qe were determined (Y. Wang et al., 2021). The kinetic parameters obtained from the models are given in Table 5. The qe and correlation coefficient (R^2) values calculated using pseudo-first order model were found to be 0.003 mg/g and 0.9792 respectively. This indicates that there is great variation between calculated (0.003 mg/g) and theoretical (14.99 mg/g) qe values. Thus the experimental data could not be well described by pseudo-first order model.

Table 5: Results of line fit model of pseudo-first order kinetic.

Pollutant	Co(mg/L)	qe,exp(mg/g	qe,cal(mg/g)	K1	R^2	Slope	Intercept
phosphate	50	14.99	0.003	-0.0304	0.9792	0.0132	-2.5832

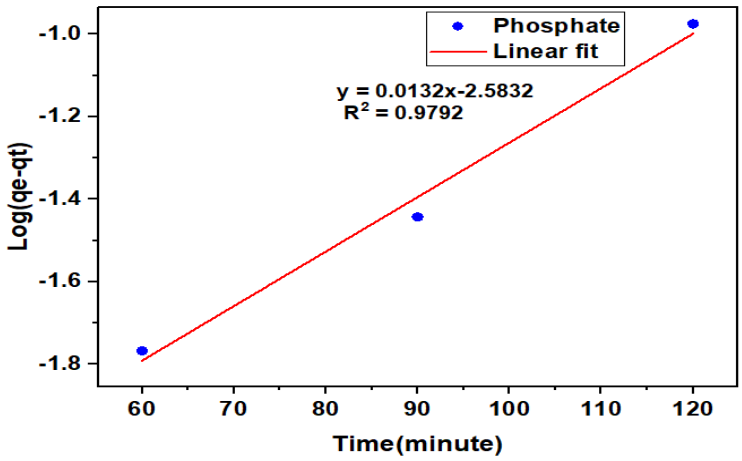

Figure 12: Pseudo-first order kinetic plot for the adsorption of phosphate ions onto $La(OH)_3@Fe_3O_4@PC$ adsorbent.

4.3.2. Pseudo-second order kinetic model

In addition to the pseudo-first-order kinetics model, the linearized form of the kinetic rate expression for a pseudo-second-order model was applied to the experimental data. Calculated equilibrium adsorption capacity q_e (cal), pseudo-second-order rate constant (K2), and the correlation coefficient (R^2) were obtained from the model using Equation 2. The linear plots of t/qt against time are shown in Figure 13 for phosphate ions adsorbed on La $(OH)_3@Fe_3O_4@PC$ adsorbent. From the slope and intercept of pseudo-second order model, t/qt versus t (Figure 13), the value of qe and K2 were determined. The kinetic parameters

obtained from the models are given in Table 5. Pseudo second-order reaction rate model which give a linear relationship adequately described the kinetics of adsorption of phosphate ions with high correlation coefficient (R^2 = 0.9999) and its theoretical equilibrium capacities qe (exp) (14.99 mg/g) fit well with the calculated qe (14.95 mg/g) data. Figure 13 and Table 6 showed the value of R^2 on pseudo-second-order for phosphate ions is higher than on pseudo-first-order kinetics and the calculated adsorption capacity qe (cal) was closer to the experimental adsorption capacity qe(exp), indicating that the pseudo-second-order kinetic model describes the adsorption process of phosphate ions by $La(OH)_3$@Fe_3O_4@PC adsorbent perfectly. This indicated that the pseudo-second-order model better represents the phosphate adsorption kinetics. A similar fit to this model has also been reported (Y. Zhang et al., 2020). Furthermore, the relatively high R^2 for the pseudo-second-order model (Table 6) indicates that the phosphate adsorption on the adsorbents was likely via chemisorption process. This observation was in agreement with the findings of other studies on phosphate adsorption by graphene−La_2O_3 composite (Chenet al., 2016), lanthanum hydroxide (Xie et al., 2014), $La(OH)_3$-modified polyacrylonitrile nanofibers (He et al., 2015) and Fe_3O_4/$La(OH)_3$ (B. Wu et al., 2017). The adsorption rate constant, K2 was determined to be 0.399 g/(mg min), which was significantly higher than those of other lanthanum-based sorbents (e.g.,0.007; 0.2198 g/(mg min)) (Ahmed & Lo, 2020).

Table 6: Results of line fit model of pseudo – second order kinetics.

Pollutant	Co(mg/L)	qe,exp(mg/g)	qe,cal(mg/g)	K2	R^2	Slope	Intercept
phosphate	50	14.99	14.95	0.399	0.9999	0.0669	0.0112

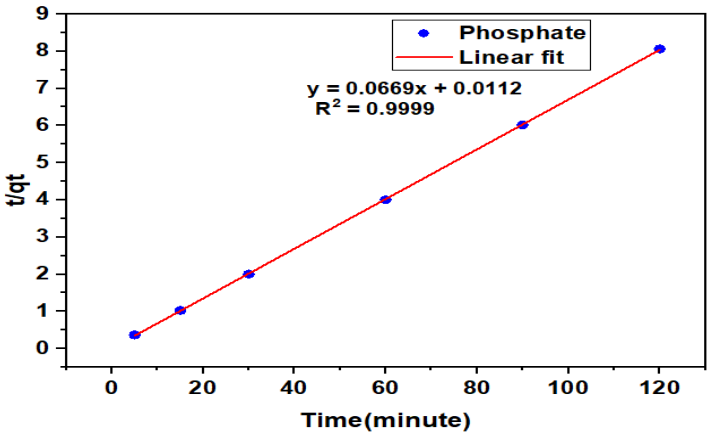

Figure 13: Pseudo-second order kinetic plot for the adsorption of phosphate ions onto $La(OH)_3@Fe_3O_4@PC$ adsorbent.

4.4. Adsorption Isotherm

The adsorption equilibrium provides important physicochemical data for evaluating the applicability of the adsorption process as a unit operation. In this study, the equilibrium data were analyzed by using Langmuir and Freundlich isotherm models. These are generally related to the type of coverage, the possibility of interaction between the adsorbent and adsorbate species, the heterogeneity and homogeneity of the adsorbent (Senthil Kumar et al., 2010). Isotherm models relate adsorbate per unit weight of adsorbent (qe) to the equilibrium adsorbate concentration in the bulk fluid phase Ce. This helps to optimize the design of an adsorption system for removal of contaminants and the selection of the appropriate adsorbent.

4.4.1. Langmuir adsorption isotherm model

From all isotherms commonly used for describing adsorption, the Langmuir adsorption isotherm model is the best known, and it has been successfully applied to various adsorption processes. The Langmuir isotherm is effective for adsorption of a solute from a liquid solution as monolayer adsorption on a surface containing a fixed number of identical sites. The experimental data were analyzed according to the linear form of the Langmuir isotherm as described in Equation 4. Figure 14 showed the experimental results obtained from the Langmuir isotherm experiment. As presented in Table 7, the correlation coefficient value (R^2 = 0.9719) indicates that the Langmuir model adequately fits to describe the equilibrium adsorption of phosphate ions onto $La(OH)_3@Fe_3O_4@PC$ adsorbent. The well-fitting of the Langmuir model also shows the presence of monolayer phosphate coverage on the

homogeneous active sites of $La(OH)_3@Fe_3O_4@PC$ adsorbent which is consistent with the pseudo-second-order model interpretation. The Langmuir model can also be used to determine the feasibility of phosphate ion adsorption onto $La(OH)_3@Fe_3O_4@PC$ adsorbent based on the R_L value which is dimensionless constant expressed in eq (5). The R_L value for the $La(OH)_3@Fe_3O_4@PC$ adsorbent in this study is 0.058, implying favorable adsorption for phosphate ions from aqueous solution (Ajmal et al., 2018; Abebe et al., 2018). The maximum phosphate adsorption capacity of the $La(OH)_3@Fe_3O_4@PC$ adsorbent determined from the Langmuir isotherm model was found to be 40.16 mg/ g.

Table 7: Summary table for the line fit graph of Langmuir isotherm model.

Pollutant	Co(mg/L)	q_e(mg/g)	Intercept	Slope	q_m(mg/g)	K_L	R_L	R^2
phosphate	50	36.04	0.0763	0.0249	40.16	0.35	0.058	0.9719

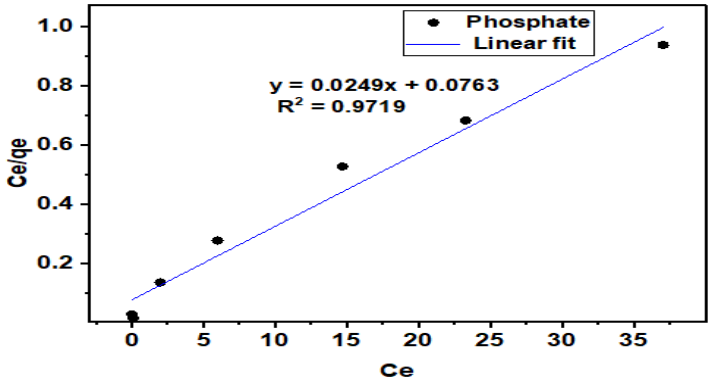

Figure 14: Langmuir adsorption isotherm model.

4.4.2. Freundlich adsorption isotherm model

The Freundlich isotherm model was the second model used to describe the adsorption data of phosphate in which the Freundlich constant K_F (mg/g), and n is characteristic constants related to the relative adsorption capacity of the adsorbent and the intensity of adsorption, respectively. The KF and 1/n can be obtained from the intercept and slope of the linear plot of Logqe versus LogCe. The Freundlich plots between Logqe versus LogCe for the adsorption of phosphate are shown in Figure 15.The applicability of the Freundlich adsorption isotherm was also analyzed, using the same set of experimental data as for the Langmuir model. The obtained n values from the Freundlich model lying between 1 and 10 (1.815) indicates the favorability of the reaction (Abebe et al., 2018). The slope (1/n) ranges between 0 and 1 and it

is a measure of adsorption intensity or surface heterogeneity. It becomes more heterogeneous as its value gets closer to zero whereas a value below 1 implies the chemisorption process as the main adsorption mechanism and above 1 is indicative of cooperative adsorption. In this study, as confirmed on the Langmuir isotherm model, being the value of 1/n closer to one (0.55) shows the homogeneous nature of the $La(OH)_3@Fe_3O_4@PC$ adsorbent surface and the type of adsorption is chemisorption process (Ajmal et al., 2018).Thus, From table 8, the Langmuir isotherm model exhibited a better mathematical fit to experimental data (R^2 = 0.9719) than the Freundlich isotherm model (R^2 = 0.8874), suggesting that the adsorption of the phosphate ions onto $La(OH)_3@Fe_3O_4@PC$ adsorbent could be favorably described by the Langmuir isotherm model. These results indicated that the adsorption process of phosphorus on the surface of $La(OH)_3@Fe_3O_4@PC$ adsorbent was the monolayer adsorption. Similar results were obtained by different studies for La-based adsorbents (Ahmed & Lo, 2020; Y. Zhang et al., 2020; Song et al., 2020).

Table 8: Result of the line fit graph of Freundlich isotherm model**.**

Pollutant	Co(mg/L)	Intercept	Slope	1/n	KF	R^2
phosphate	50	0.8757	0.5511	0.55	7.511	0.8874

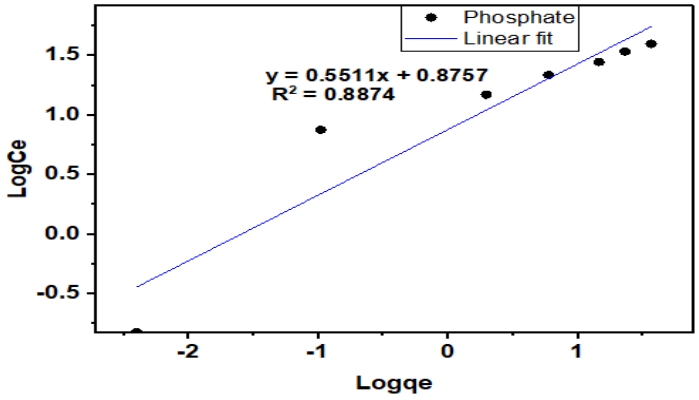

Figure 15: Freundlich adsorption isotherm model.

4.5. Phosphate Removal from ASTU WWTP Effluent Result

The initial concentration of phosphate in the wastewater sample was measured and found to be 3.729 mg/L. The $La(OH)_3@Fe_3O_4@PC$ adsorbent effectively removed the phosphate ion contaminants from the real wastewater samples with 98% adsorption efficiency, as can be seen in table 9.

Table 9: Adsorption studies on removal of phosphate from wastewater sample

Wastewater sample pollutant	Co(mg/L)	pH	Dose of adsorbent(g/L)	Contact time(min)	Ce(mg/L)	% Removal
phosphate	3.729	5	0.2	30	0.05877	98.424

4.6. Recyclability of $La(OH)_3@Fe_3O_4@PC$ Adsorbent

Due to its magnetic property, the synthesized nanocomposite can be used for several times by separating the used adsorbent using external magnet and washing it by deionized water. Re-usability of the $La(OH)_3@Fe_3O_4@PC$ nanocomposite was assessed for six consecutive phosphate adsorption cycles. The desorption process for the phosphate previously adsorbed on the $La(OH)_3@Fe_3O_4@PC$ composites was optimized to be able to reuse the nanoadsorbents for further adsorption process and to recover the phosphate. The average desorption efficiency of the adsorbent was found to be about 81.37% which indicates that the adsorption of phosphate on the adsorbent involves physical in addition to chemical adsorption process. Figure 16 and Table 10 showed the removal efficiency for each cycles for $La(OH)_3@Fe_3O_4@PC$ adsorbent using the desorption solution. There was a gradual decrease in phosphate removal efficiencies with an increasing number of cycles as shown in Figure 16. The removal efficiencies of phosphate for 1, 2, 3, 4, 5, and 6 cycles were found to be 99.79%, 95.93, 93.24%, 88.71%, 86.55%, and 82.86% respectively. Hence, the phosphate uptake capacity on the $La(OH)_3@Fe_3O_4@PC$ adsorbent was reduced as the number of cycles increase. The regeneration experiments presented in Figure 16 showed that the $La(OH)_3@Fe_3O_4@PC$ adsorbent could be reused repeatedly in the adsorption and removal of phosphate ions without significantly losing the adsorption property. Similar results were reported by different studies (Y. Zhang et al., 2020;B. Wu et al., 2017).

Table 10: Recyclability of $La(OH)_3@Fe_3O_4@PC$ adsorbent for phosphate removal

Cycle	Co(mg/L)	Ce(mg/L)	% Removal
1	50	0.105	99.79
2	50	2.035	95.93
3	50	3.381	93.24
4	50	5.643	88.71
5	50	6.725	86.55
6	50	8.570	82.86

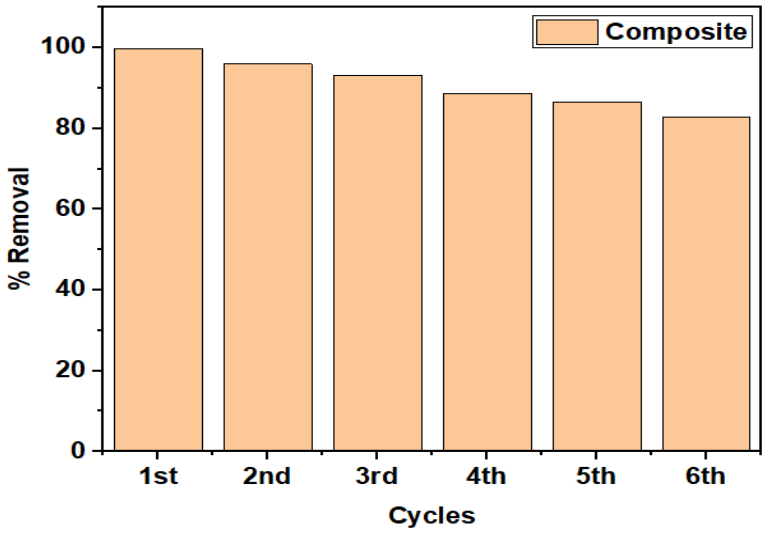

Figure 16: Recyclability of $La(OH)_3@Fe_3O_4@PC$ adsorbent for phosphate removal.

5. CONCLUSION AND RECOMMENDATION

5.1. Conclusion

This study examined the removal of phosphate ions from wastewater by using highly efficient adsorbent, $La(OH)_3@Fe_3O_4@PC$. The magnetically recyclable $La(OH)_3@Fe_3O_4@PC$ nanocomposite was successfully developed through a low-temperature green synthesis route, which offers an advantage of a simple synthesis procedure. XRD and SEM characterization results have confirmed the successful loading of magnetite and lanthanum hydroxide onto the porous carbon structure. The phosphate adsorption capacities of the synthesized $La(OH)_3@Fe_3O_4@PC$ nanocomposite was investigated. The pseudo-second-order and Langmuir isotherm models were shown the best to describe the phosphate removal, with a maximum capacity of 40.16 mg/g at pH 5. Moreover, 0.2 g/L dosage of the $La(OH)_3@Fe_3O_4@PC$ nanocomposite has shown to be capable of removing 98.42% of the phosphate ions from wastewater. $La(OH)_3@Fe_3O_4@PC$ nanocomposite also exhibited good magnetic property for easy recovery, excellent recyclability and environmental friendliness. Further, phosphate adsorbed onto the $La(OH)_3@Fe_3O_4@PC$ nanocomposite can easily be eluted by using sodium hydroxide solution. The nanocomposite has shown excellent reusability for six consecutive adsorption-desorption cycles. Taken together, these properties show the potential applicability of using the $La(OH)_3@Fe_3O_4@PC$ nanocomposite materials to remove phosphate from treated wastewater effluent.

5.2. Recommendation

Because of its time saving, simplicity, low cost, and green technology, it is better for researcher to further studies on $La(OH)_3@Fe_3O_4@PC$ nanocomposites for phosphate removal from wastewaters. It is also possible to study the efficiency of the desorption process by using different eluent to get a full picture of the removal capacity of the $La(OH)_3@Fe_3O_4@PC$ nanocomposite for phosphate and other pollutants removal from different types of wastewater. The multifunctional properties of the $La(OH)_3@Fe_3O_4@PC$ adsorbent beyond adsorption of phosphate should be investigated like metal ions removal from seawater and humic substances, naturally occurring organic polymeric compounds widely distributed in wastewater. The Lanthanum and iron release from such adsorbent during

phosphate adsorption at certain pH conditions must be given due attention as different studies confirmed this cases. In addition to that although the $La(OH)_3@Fe_3O_4@PC$ adsorbent is highly efficient in reducing phosphate concentrations to trace levels, there are still some limitations that inhibit the wide application. For example, the $La(OH)_3@Fe_3O_4@PC$ adsorbent exhibit high phosphate adsorption capacity under acidic conditions. Thus its performance will be greatly reduced when wastewater effluents are under neutral and alkaline conditions.

Therefore, we recommended that for a researcher it is better to assess by expanding this study to obtain new lanthanum-based adsorbents with enhanced phosphate adsorption capabilities over a wider pH range, easy synthesis method and separation techniques to overcome these disadvantages.

6. REFERENCE

Abdul Salim, N. A., Abdullah, N. H., Khairuddin, M. R., Rudie Arman, M. A. B. Z., Khamidun, M. H., Fulazzaky, M. A., Mohd Yusoff, A. R., Othman, M. H. D., & Puteh, M. H. (2018). Adsorption of phosphate from aqueous solutions using waste mussel shell. *MATEC Web of Conferences*, *250*, *456-487*. https://doi.org/10.1051/matecconf/201825006013

Abebe, B., Taddesse, A. M., Kebede, T., Teju, E., & Diaz, I. (2017). Fe-Al-Mn ternary oxide nanosorbent: Synthesis, characterization and phosphate sorption property. *Journal of Environmental Chemical Engineering*, *5*(2), 1330–1340. https://doi.org/10.1016/j.jece.2017.02.026

Aghazadeh, M., Golikand, A. N., Ghaemi, M., & Yousefi, T. (2011). A novel lanthanum hydroxide nanostructure prepared by cathodic electrodeposition. *Materials Letters*, *65*(10), 1466–1468. https://doi.org/10.1016/j.matlet.2011.02.039

Ahmad, I. Z., Ahmad, A., Tabassum, H., & Kuddus, M. (2019). Applications of nanoparticles in the treatment of wastewater. *Handbook of Ecomaterials*, *1*, 275–299. https://doi.org/10.1007/978-3-319-68255-6_37

Ahmed, S., Ashiq, M. N., Li, D., Tang, P., Leroux, F., & Feng, Y. (2019). Recent Progress on Adsorption Materials for Phosphate Removal. *Recent Patents on Nanotechnology*, *13*(1), 3–16. https://doi.org/10.2174/1872210513666190306155245

Ahmed, S., & Lo, I. M. C. (2020). Phosphate removal from river water using a highly efficient magnetically recyclable Fe3O4/La(OH)3 nanocomposite. *Chemosphere*, *261*, 128118. https://doi.org/10.1016/j.chemosphere.2020.128118

Ahmed, S., Zhang, Y., Wu, B., Zheng, Z., Leung, C. F., Choy, T. yip, Kwok, Y. ting, & Lo, I. M. C. (2021). Scaled-up development of magnetically recyclable Fe3O4/La(OH)3 composite for river water phosphate removal: From bench-scale to pilot-scale study. *Science of the Total Environment*, *791*, 148281. https://doi.org/10.1016/j.scitotenv.2021.148281

Ajmal, Z., Muhmood, A., Usman, M., Kizito, S., Lu, J., Dong, R., & Wu, S. (2018). Phosphate removal from aqueous solution using iron oxides : adsorption , desorption and regeneration characteristics. *Journal of Colloid And Interface Science*. https://doi.org/10.1016/j.jcis.2018.05.084

Anuradha, J., Abbasi, T., & Abbasi, S. A. (2015). An eco-friendly method of synthesizing gold nanoparticles using an otherwise worthless weed pistia (Pistia stratiotes L.). *Journal of Advanced Research*, *6*(5), 711–720. https://doi.org/10.1016/j.jare.2014.03.006

Awual, M. R. (2019). Efficient phosphate removal from water for controlling eutrophication using novel composite adsorbent. *Journal of Cleaner Production*, *228*, 1311–1319. https://doi.org/10.1016/j.jclepro.2019.04.325

Ayawei, N., Ebelegi, A. N., & Wankasi, D. (2017). Modelling and Interpretation of Adsorption Isotherms. *Journal of Chemistry*, *2017*. https://doi.org/10.1155/2017/3039817

Basheer, A. A. (2018). New generation nano-adsorbents for the removal of emerging contaminants in water. *Journal of Molecular Liquids*, *261*, 583–593. https://doi.org/10.1016/j.molliq.2018.04.021

Batool, F., Akbar, J., Iqbal, S., Noreen, S., & Bukhari, S. N. A. (2018). Study of Isothermal, Kinetic, and Thermodynamic Parameters for Adsorption of Cadmium: An Overview of Linear and Nonlinear Approach and Error Analysis. *Bioinorganic Chemistry and Applications*, *2018*. https://doi.org/10.1155/2018/3463724

Bilgiç, A., & Çimen, A. (2019). Removal of chromium(vi) from polluted wastewater by chemical modification of silica gel with 4-acetyl-3-hydroxyaniline. *RSC Advances*, *9*(64), 37403–37414. https://doi.org/10.1039/c9ra05810a

Bowes, M. J., Jarvie, H. P., Halliday, S. J., Skeffington, R. A., Wade, A. J., Loewenthal, M., Gozzard, E., Newman, J. R., & Palmer-Felgate, E. J. (2015). Characterising phosphorus and nitrate inputs to a rural river using high-frequency concentration-flow relationships. *Science of the Total Environment*, *511*, 608–620. https://doi.org/10.1016/j.scitotenv.2014.12.086

Bruun, C., Lu, C., Klementiev, K., Hassenkam, T., Qian, W., & Ai, J. (2021). *High affinity lanthanum doped iron oxide nanosheets for phosphate removal Publication date : Publisher ' s PDF , also known as Version of record Citation for published version (APA): High affinity lanthanum doped iron oxide nanosheets for phosphate remo*. https://doi.org/10.1016/j.cej.2021.130009

Buketov, A. V., Sapronov, O. O., & Brailo, M. V. (2014). Investigation of the Physico-Mechanical and Thermophysical Properties of Epoxy Composites with a Two-Component Bidisperse Filler. *Strength of Materials*, *46*(5), 717–723. https://doi.org/10.1007/s11223-014-9605-z

Carlos, L., Garcia Einschlag, F. S., C., M., & O., D. (2013). Applications of Magnetite Nanoparticles for Heavy Metal Removal from Wastewater. *Waste Water - Treatment Technologies and Recent Analytical Developments*. https://doi.org/10.5772/54608

Chaudhary, R., Nawaz, K., Khan, A. K., Hano, C., Abbasi, B. H., & Anjum, S. (2020). An overview of the algae-mediated biosynthesis of nanoparticles and their biomedical applications. *Biomolecules*, *10*(11), 1–35. https://doi.org/10.3390/biom10111498

Chen, B., Chen, Z., & Lv, S. (2011). A novel magnetic biochar efficiently sorbs organic pollutants and phosphate. *Bioresource Technology*, *102*(2), 716–723. https://doi.org/10.1016/j.biortech.2010.08.067

Chen, L., Li, Y., Sun, Y., Chen, Y., & Qian, J. (2019). La(OH)3 loaded magnetic mesoporous nanospheres with highly efficient phosphate removal properties and superior pH stability. *Chemical Engineering Journal*, *360*, 342–348. https://doi.org/10.1016/j.cej.2018.11.234

Chen, Y., Xu, R., Li, Y., Liu, Y., Wu, Y., Chen, Y., Zhang, J., Chen, S., Yin, H., Zeng, Z., Wang, S., & Peng, Z. (2020). La(OH)3-modified magnetic CoFe2O4 nanocomposites: A novel adsorbent with highly efficient activity and reusability for phosphate removal. *Colloids and Surfaces A: Physicochemical and Engineering Aspects*, *599*(May), 1–11. https://doi.org/10.1016/j.colsurfa.2020.124870

Cheng, W., Zhang, W., Hu, L., Ding, W., Wu, F., & Li, J. (2016). Etching synthesis of iron oxide nanoparticles for adsorption of arsenic from water. *RSC Advances*, *6*(19), 15900–15910. https://doi.org/10.1039/c5ra26143k

Cheriyamundath, S., & Vavilala, S. L. (2021). Nanotechnology-based wastewater treatment. *Water and Environment Journal*, *35*(1), 123–132. https://doi.org/10.1111/wej.12610

Coates, J. (2006). Interpretation of Infrared Spectra, A Practical Approach. *Encyclopedia of Analytical Chemistry*, 1–23. https://doi.org/10.1002/9780470027318.a5606

Crini, G., Lichtfouse, E., Wilson, L. D., & Morin-Crini, N. (2019). Conventional and non-conventional adsorbents for wastewater treatment. *Environmental Chemistry Letters*, *17*(1), 195–213. https://doi.org/10.1007/s10311-018-0786-8

Dai, L., Wu, B., Tan, F., He, M., Wang, W., Qin, H., Tang, X., Zhu, Q., Pan, K., & Hu, Q. (2014). Engineered hydrochar composites for phosphorus removal/recovery: Lanthanum doped hydrochar prepared by hydrothermal carbonization of lanthanum pretreated rice straw. *Bioresource Technology*, *161*, 327–332. https://doi.org/10.1016/j.biortech.2014.03.086

Daneshvar Tarigh, G., & Shemirani, F. (2013). Magnetic multi-wall carbon nanotube nanocomposite as an adsorbent for preconcentration and determination of lead (II) and manganese (II) in various matrices. *Talanta*, *115*, 744–750. https://doi.org/10.1016/j.talanta.2013.06.018

Deliyanni, E. A., Peleka, E. N., & Lazaridis, N. K. (2007). Comparative study of phosphates removal from aqueous solutions by nanocrystalline akaganéite and hybrid surfactant-akaganéite. *Separation and Purification Technology*, *52*(3), 478–486. https://doi.org/10.1016/j.seppur.2006.05.028

Dong, H., Wei, L., & Tarpeh, W. A. (2020). Electro-assisted regeneration of pH-sensitive ion exchangers for sustainable phosphate removal and recovery. *Water Research*, *184*, 116167. https://doi.org/10.1016/j.watres.2020.116167

Dong, S., Wang, Y., Zhao, Y., Zhou, X., & Zheng, H. (2017). La3+/La(OH)3 loaded magnetic cationic hydrogel composites for phosphate removal: Effect of lanthanum species and mechanistic study. *Water Research*, *126*, 433–441. https://doi.org/10.1016/j.watres.2017.09.050

El-sayed, M. E. A. (2020). Nanoadsorbents for water and wastewater remediation. *Science of the Total Environment*, *739*, 139903. https://doi.org/10.1016/j.scitotenv.2020.139903

Fang, L., Liu, R., Li, J., Xu, C., Huang, L. Z., & Wang, D. (2018). Magnetite/Lanthanum hydroxide for phosphate sequestration and recovery from lake and the attenuation effects of sediment particles. *Water Research*, *130*, 243–254. https://doi.org/10.1016/j.watres.2017.12.008

Fang, L., Shi, Q., Nguyen, J., Wu, B., Wang, Z., & Lo, I. M. C. (2017). Removal Mechanisms of Phosphate by Lanthanum Hydroxide Nanorods: Investigations using EXAFS, ATR-FTIR, DFT, and Surface Complexation Modeling Approaches. *Environmental Science and Technology*, *51*(21), 12377–12384. https://doi.org/10.1021/acs.est.7b03803

Fu, H., Yang, Y., Zhu, R., Liu, J., Usman, M., Chen, Q., & He, H. (2018a). Superior adsorption of phosphate by ferrihydrite-coated and lanthanum-decorated magnetite. *Journal of Colloid and Interface Science*, *530*, 704–713. https://doi.org/10.1016/j.jcis.2018.07.025

Fu, H., Yang, Y., Zhu, R., Liu, J., Usman, M., Chen, Q., & He, H. (2018b). Superior adsorption of phosphate by ferrihydrite-coated and lanthanum-decorated magnetite. *Journal of Colloid and Interface Science*, *530*, 704–713. https://doi.org/10.1016/j.jcis.2018.07.025

Gatoo, M. A., Naseem, S., Arfat, M. Y., Mahmood Dar, A., Qasim, K., & Zubair, S. (2014). Physicochemical properties of nanomaterials: Implication in associated toxic manifestations. *BioMed Research International*, *2014*. https://doi.org/10.1155/2014/498420

Gupta, N., Pant, P., Gupta, C., Goel, P., Jain, A., Anand, S., & Pundir, A. (2018). Engineered magnetic nanoparticles as efficient sorbents for wastewater treatment: a review. *Materials Research Innovations*, *22*(7), 434–450. https://doi.org/10.1080/14328917.2017.1334846

Gusain, R., Kumar, N., & Ray, S. S. (2020). Recent advances in carbon nanomaterial-based adsorbents for water purification. *Coordination Chemistry Reviews*, *405*, 213111. https://doi.org/10.1016/j.ccr.2019.213111

He, Y., Lin, H., Dong, Y., & Wang, L. (2017). Preferable adsorption of phosphate using lanthanum-incorporated porous zeolite: Characteristics and mechanism. *Applied Surface Science*, *426*, 995–1004. https://doi.org/10.1016/j.apsusc.2017.07.272

Hu, Q., & Zhang, Z. (2019). Application of Dubinin–Radushkevich isotherm model at the solid/solution interface: A theoretical analysis. *Journal of Molecular Liquids*, *277*, 646–648. https://doi.org/10.1016/j.molliq.2019.01.005

Huang, W. Y., Li, D., Liu, Z. Q., Tao, Q., Zhu, Y., Yang, J., & Zhang, Y. M. (2014). Kinetics, isotherm, thermodynamic, and adsorption mechanism studies of La(OH)3-modified exfoliated vermiculites as highly efficient phosphate adsorbents. *Chemical Engineering Journal*, *236*, 191–201. https://doi.org/10.1016/j.cej.2013.09.077

Huang, W., Yu, X., Tang, J., Zhu, Y., Zhang, Y., & Li, D. (2015). Enhanced adsorption of phosphate by flower-like mesoporous silica spheres loaded with lanthanum. *Microporous and Mesoporous Materials*, *217*, 225–232. https://doi.org/10.1016/j.micromeso.2015.06.031

Ijaz, I., Gilani, E., Nazir, A., & Bukhari, A. (2020). Detail review on chemical, physical and green synthesis, classification, characterizations and applications of nanoparticles. *Green Chemistry Letters and Reviews*, *13*(3), 59–81. https://doi.org/10.1080/17518253.2020.1802517

Ismail, L., Khalili, F., & Abu Orabi, F. M. (2020). Modification of Silica Nanoparticles with Cysteine or Methionine Amino Acids for the Removal of Uranium (VI) from Aqueous Solution. *Silicon*, *12*(11), 2647–2661. https://doi.org/10.1007/s12633-019-00361-9

Joshi, S., Sharma, M., Kumari, A., Shrestha, S., & Shrestha, B. (2019). Arsenic removal fromwater by adsorption onto iron oxide/nano-porous carbon magnetic composite. *Applied Sciences (Switzerland)*, *9*(18). https://doi.org/10.3390/app9183732

Koilraj, P., & Sasaki, K. (2017). Selective removal of phosphate using La-porous carbon composites from aqueous solutions: Batch and column studies. *Chemical Engineering Journal*, *317*, 1059–1068. https://doi.org/10.1016/j.cej.2017.02.075

Kumar, L., Alam, M. S., Meena, C. L., Jain, R., & Bansal, A. K. (2009). Chapter 4 Fexofenadine Hydrochloride. In *Profiles of Drug Substances, Excipients and Related Methodology* (1st ed., Vol. 34, Issue 08). Elsevier Inc. https://doi.org/10.1016/S1871-5125(09)34004-2

Kuroki, V., Bosco, G. E., Fadini, P. S., Mozeto, A. A., Cestari, A. R., & Carvalho, W. A. (2014). Use of a La(III)-modified bentonite for effective phosphate removal from aqueous media. *Journal of Hazardous Materials*, *274*, 124–131. https://doi.org/10.1016/j.jhazmat.2014.03.023

Lai, L., Xie, Q., Chi, L., Gu, W., & Wu, D. (2016). Adsorption of phosphate from water by easily separable Fe3O4@SiO2 core/shell magnetic nanoparticles functionalized with hydrous lanthanum oxide. *Journal of Colloid and Interface Science*, *465*, 76–82. https://doi.org/10.1016/j.jcis.2015.11.043

Lencha, S. M., Tränckner, J., & Dananto, M. (2021). Assessing the water quality of lake hawassa Ethiopia—Trophic state and suitability for anthropogenic uses—applying common water quality indices. *International Journal of Environmental Research and Public Health*, *18*(17). https://doi.org/10.3390/ijerph18178904

Li, M., Liu, J., Xu, Y., & Qian, G. (2016). *Phosphate adsorption on metal oxides and metal hydroxides : A comparative review*. *332*(May), 319–332.

Limousin, G., Gaudet, J. P., Charlet, L., Szenknect, S., Barthès, V., & Krimissa, M. (2007). Sorption isotherms: A review on physical bases, modeling and measurement. *Applied Geochemistry*, *22*(2), 249–275. https://doi.org/10.1016/j.apgeochem.2006.09.010

Lin, Z., & Chen, J. (2021). Magnetic Fe3O4@MgAl-LDH@La(OH)3 composites with a hierarchical core-shell structure for phosphate removal from wastewater and inhibition of labile sedimentary phosphorus release. *Chemosphere*, *264*, 128551. https://doi.org/10.1016/j.chemosphere.2020.128551

Liu, B., Yu, Y., Han, Q., Lou, S., Zhang, L., & Zhang, W. (2020). Fast and efficient phosphate removal on lanthanum-chitosan composite synthesized by controlling the amount of cross-linking agent. *International Journal of Biological Macromolecules*, *157*, 247–258. https://doi.org/10.1016/j.ijbiomac.2020.04.159

Liu, S. J., Li, J., Yang, Y. K., Wang, J., & Ding, H. (2016). Influence of environmental factors on the phosphorus adsorption of lanthanum-modified bentonite in eutrophic water and sediment. *Environmental Science and Pollution Research*, *23*(3), 2487–2494. https://doi.org/10.1007/s11356-015-5453-z

Liu, X., Zong, E., Hu, W., Song, P., Wang, J., Liu, Q., Ma, Z., & Fu, S. (2019). Lignin-Derived Porous Carbon Loaded with La(OH) 3 Nanorods for Highly Efficient Removal of Phosphate. *ACS Sustainable Chemistry and Engineering*, *7*(1), 758–768. https://doi.org/10.1021/acssuschemeng.8b04382

Lu, C., Klementiev, K., Hassenkam, T., Qian, W., Ai, J., & Chr. Bruun Hansen, H. (2021). High affinity lanthanum doped iron oxide nanosheets for phosphate removal. *Chemical Engineering Journal*, *422*(March), 130009. https://doi.org/10.1016/j.cej.2021.130009

Luo, Y., Xie, K., Feng, Y., He, Q., Zhang, K., & Shen, S. (2021). Colloids and Surfaces A : Physicochemical and Engineering Aspects Synthesis of a La (OH) 3 nanorod / walnut shell biochar composite for reclaiming phosphate from aqueous solutions. *Colloids and Surfaces A: Physicochemical and Engineering Aspects*, *610*(August 2020), 125736. https://doi.org/10.1016/j.colsurfa.2020.125736

Macys, J. J. (2005). On estimates of factorial quotients. *Lithuanian Mathematical Journal*, *45*(3), 284–291. https://doi.org/10.1007/s10986-005-0030-7

Makita, Y., Sonoda, A., Sugiura, Y., Ogata, A., Suh, C., Lee, J. hoon, & Ooi, K. (2020). Phosphorus removal from model wastewater using lanthanum hydroxide microcapsules with poly(vinyl chloride) shells. *Separation and Purification Technology*, *241*(September 2019), 116707. https://doi.org/10.1016/j.seppur.2020.116707

Manchisi, J., Matinde, E., Rowson, N. A., Simmons, M. J. H., Simate, G. S., Ndlovu, S., & Mwewa, B. (2020). Ironmaking and Steelmaking Slags As Sustainable Adsorbents For Industrial Effluents And Wastewater Treatment: A critical review of properties, performance, challenges and opportunities. *Sustainability (Switzerland)*, *12*(5), 1–47. https://doi.org/10.3390/su12052118

Mani, T., Murugan, P., Abedi, J., & Mahinpey, N. (2010). Pyrolysis of wheat straw in a thermogravimetric analyzer: Effect of particle size and heating rate on devolatilization and estimation of global kinetics. *Chemical Engineering Research and Design*, *88*(8), 952–958. https://doi.org/10.1016/j.cherd.2010.02.008

Mazloumi, M., Shahcheraghi, N., Kajbafvala, A., Zanganeh, S., Lak, A., Mohajerani, M. S., & Sadrnezhaad, S. K. (2009). 3D bundles of self-assembled lanthanum hydroxide nanorods via a rapid microwave-assisted route. *Journal of Alloys and Compounds*, *473*(1–2), 283–287. https://doi.org/10.1016/j.jallcom.2008.05.052

Mekonnen, D. T., Alemayehu, E., & Lennartz, B. (2020). Removal of phosphate ions from aqueous solutions by adsorption onto leftover coal. *Water (Switzerland)*, *12*(5), 1–15. https://doi.org/10.3390/W12051381

Muniz, F. T. L., Miranda, M. A. R., Morilla Dos Santos, C., & Sasaki, J. M. (2016). The Scherrer equation and the dynamical theory of X-ray diffraction. *Acta Crystallographica Section A: Foundations and Advances*, *72*(3), 385–390. https://doi.org/10.1107/S205327331600365X

Nayak, D., Pradhan, S., Ashe, S., Rauta, P. R., & Nayak, B. (2015). Biologically synthesised silver nanoparticles from three diverse family of plant extracts and their anticancer activity against epidermoid A431 carcinoma. *Journal of Colloid and Interface Science*, *457*, 329–338. https://doi.org/10.1016/j.jcis.2015.07.012

Pratiwi, D., Prasetyo, D. J., & Poeloengasih, C. D. (2019). Adsorption of Methylene Blue dye using Marine algae Ulva lactuca. *IOP Conference Series: Earth and Environmental Science*, *251*(1). https://doi.org/10.1088/1755-1315/251/1/012012

Qiu, H., Lv, L., Pan, B. C., Zhang, Q. J., Zhang, W. M., & Zhang, Q. X. (2009). Critical review in adsorption kinetic models. *Journal of Zhejiang University: Science A*, *10*(5), 716–724. https://doi.org/10.1631/jzus.A0820524

Rahman, S., Navarathna, C. M., Krishna Das, N., Alchouron, J., Reneau, P., Stokes, S., V.K.G. Thirumalai, R., Perez, F., Barbary Hassan, E., Mohan, D., Pittman, C. U., & Mlsna, T. (2021). High capacity aqueous phosphate reclamation using Fe/Mg-layered double hydroxide (LDH) dispersed on biochar. *Journal of Colloid and Interface Science*, *597*, 182–195. https://doi.org/10.1016/j.jcis.2021.03.114

Ramos Filho, F. G., Mélo, T. J. A., Rabello, M. S., & Silva, S. M. L. (2005). Thermal stability of nanocomposites based on polypropylene and bentonite. *Polymer Degradation and Stability*, *89*(3), 383–392. https://doi.org/10.1016/j.polymdegradstab.2004.12.011

Rashid, R., Shafiq, I., Akhter, P., Iqbal, M. J., & Hussain, M. (2021). A state-of-the-art review on wastewater treatment techniques: the effectiveness of adsorption method. *Environmental Science and Pollution Research*, *28*(8), 9050–9066. https://doi.org/10.1007/s11356-021-12395-x

Razanajatovo, M. R., Gao, W., Song, Y., Zhao, X., Sun, Q., & Zhang, Q. (2021). Selective adsorption of phosphate in water using lanthanum-based nanomaterials: A critical review. *Chinese Chemical Letters*, *32*(9), 2637–2647. https://doi.org/10.1016/j.cclet.2021.01.046

Saadatkhah, N., Carillo Garcia, A., Ackermann, S., Leclerc, P., Latifi, M., Samih, S., Patience, G. S., & Chaouki, J. (2020). Experimental methods in chemical engineering: Thermogravimetric analysis—TGA. *Canadian Journal of Chemical Engineering*, *98*(1), 34–43. https://doi.org/10.1002/cjce.23673

Sengupta, S., & Pandit, A. (2011). Selective removal of phosphorus from wastewater combined with its recovery as a solid-phase fertilizer. *Water Research*, *45*(11), 3318–3330. https://doi.org/10.1016/j.watres.2011.03.044

Senthil Kumar, P., Vincent, C., Kirthika, K., & Sathish Kumar, K. (2010). Kinetics and equilibrium studies of Pb2+ ion removal from aqueous solutions by use of nano-silversol-coated activated carbon. *Brazilian Journal of Chemical Engineering*, *27*(2), 339–346. https://doi.org/10.1590/s0104-66322010000200012

Sharma, A., Sharma, S., Sharma, K., Chetri, S. P. K., Vashishtha, A., Singh, P., Kumar, R., Rathi, B., & Agrawal, V. (2016). Algae as crucial organisms in advancing nanotechnology: a systematic review. *Journal of Applied Phycology*, *28*(3), 1759–1774. https://doi.org/10.1007/s10811-015-0715-1

Simonin, J. P. (2016). On the comparison of pseudo-first order and pseudo-second order rate laws in the modeling of adsorption kinetics. *Chemical Engineering Journal*, *300*, 254–263. https://doi.org/10.1016/j.cej.2016.04.079

Sinha, S. N., Paul, D., Halder, N., Sengupta, D., & Patra, S. K. (2015). Green synthesis of silver nanoparticles using fresh water green alga Pithophora oedogonia (Mont.) Wittrock and evaluation of their antibacterial activity. *Applied Nanoscience (Switzerland)*, *5*(6), 703–709. https://doi.org/10.1007/s13204-014-0366-6

Song, Q., Huang, S., Xu, L., Wang, N., Hu, Z., Luo, X., & Zheng, Z. (2020). Synthesis of magnetite/lanthanum hydroxide composite and magnetite/aluminum hydroxide composite for removal of phosphate. *Science of the Total Environment*, *723*. https://doi.org/10.1016/j.scitotenv.2020.137838

Swenson, H., & Stadie, N. P. (2019). Langmuir's Theory of Adsorption: A Centennial Review [Review-article]. *Langmuir*, *35*, 5409–5426. https://doi.org/10.1021/acs.langmuir.9b00154

Taffese, T., Tilahun, S., & Steenhuis, T. (2014). Phosphorus Modeling, in Lake Tana Basin, Ethiopia. *Journal of Environment and Human*, *2014*(2), 47–55. https://doi.org/10.15764/eh.2014.02007

Viju Kumar, V. G., & Prem, A. A. (2018). Green synthesis and characterization of iron oxide nanoparticles using phyllanthus niruri extract. *Oriental Journal of Chemistry*, *34*(5), 2583–2589. https://doi.org/10.13005/ojc/340547

Vikrant, K., & Kim, K. (2018). Nanomaterials for the adsorptive treatment of Hg(II) ions from water. *Chemical Engineering Journal*, *October*. https://doi.org/10.1016/j.cej.2018.10.022

Wang, P., Armutlulu, A., Jiang, W., Lai, B., & Xie, R. (2019). *La @ Fe / C composites from ilmenite for e ffi cient phosphate removal from aqueous solution †*. 28312–28322. https://doi.org/10.1039/c9ra05606h

Wang, Y., Li, J., Yuan, Y., Si, Y., Xu, J., Li, M., & Peng, X. (2021a). La(OH)3 loaded magnetic nanocomposites derived from sugarcane bagasse cellulose for phosphate adsorption: Characterization, performance and mechanism. *Colloids and Surfaces A: Physicochemical and Engineering Aspects*, *626*(May), 127060. https://doi.org/10.1016/j.colsurfa.2021.127060

Wang, Y., Li, J., Yuan, Y., Si, Y., Xu, J., Li, M., & Peng, X. (2021b). La(OH)3 loaded magnetic nanocomposites derived from sugarcane bagasse cellulose for phosphate adsorption: Characterization, performance and mechanism. *Colloids and Surfaces A: Physicochemical and Engineering Aspects*, *626*(May), 127060. https://doi.org/10.1016/j.colsurfa.2021.127060

Wang, Z., Xu, C., Li, X., & Liu, Z. (2015). In situ green synthesis of Ag nanoparticles on tea polyphenols-modified graphene and their catalytic reduction activity of 4-nitrophenol. *Colloids and Surfaces A: Physicochemical and Engineering Aspects*, *485*, 102–110. https://doi.org/10.1016/j.colsurfa.2015.09.015

Wu, B., Fang, L., Fortner, J. D., Guan, X., & Lo, I. M. C. (2017). Highly efficient and selective phosphate removal from wastewater by magnetically recoverable La(OH)3/Fe3O4 nanocomposites. *Water Research*, *126*, 179–188. https://doi.org/10.1016/j.watres.2017.09.034

Wu, W., & Maravelias, C. T. (2019). Identifying the Characteristics of Promising Renewable Replacement Chemicals. *IScience*, *15*. https://doi.org/10.1016/j.isci.2019.04.012

Xiao, J. D., Qiu, L. G., Jiang, X., Zhu, Y. J., Ye, S., & Jiang, X. (2013). Magnetic porous carbons with high adsorption capacity synthesized by a microwave-enhanced high temperature ionothermal method from a Fe-based metal-organic framework. *Carbon*, *59*, 372–382. https://doi.org/10.1016/j.carbon.2013.03.032

Xiao, X., Huang, Y., & Dong, F. (2014). *Synthesis and Application of One-Dimensional La (OH) 3 Nanostructures : An Overview*. *2014*(Iii).

Xie, J., Lin, Y., Li, C., Wu, D., & Kong, H. (2015). Removal and recovery of phosphate from water by activated aluminum oxide and lanthanum oxide. *Powder Technology*, *269*, 351–357. https://doi.org/10.1016/j.powtec.2014.09.024

Xie, J., Wang, Z., Lu, S., Wu, D., Zhang, Z., & Kong, H. (2014). Removal and recovery of phosphate from water by lanthanum hydroxide materials. *Chemical Engineering Journal*, *254*, 163–170. https://doi.org/10.1016/j.cej.2014.05.113

Yang, H., Masse, S., Rouelle, M., Aubry, E., Li, Y., Roux, C., Journaux, Y., Li, L., & Coradin, T. (2015). Magnetically recoverable iron oxide–hydroxyapatite nanocomposites for lead removal. *International Journal of Environmental Science and Technology*, *12*(4), 1173–1182. https://doi.org/10.1007/s13762-014-0514-2

Yao, H., Dai, Q., & You, Z. (2015). Fourier Transform Infrared Spectroscopy characterization of aging-related properties of original and nano-modified asphalt binders. *Construction and Building Materials*, *101*(Md), 1078–1087. https://doi.org/10.1016/j.conbuildmat.2015.10.085

Yew, Y. P., Shameli, K., Miyake, M., Kuwano, N., Bt Ahmad Khairudin, N. B., Bt Mohamad, S. E., & Lee, K. X. (2016). Green Synthesis of Magnetite (Fe3O4) Nanoparticles Using Seaweed (Kappaphycus alvarezii) Extract. *Nanoscale Research Letters*, *11*(1). https://doi.org/10.1186/s11671-016-1498-2

Yuvakkumar, R., & Hong, S. I. (2014). Green synthesis of spinel magnetite iron oxide nanoparticles. *Advanced Materials Research*, *1051*, 39–42. https://doi.org/10.4028/www.scientific.net/AMR.1051.39

Zhang, K., Zuo, W., Wang, Z., Liu, J., Li, T., Wang, B., & Yang, Z. (2015). A simple route to CoFe2O4 nanoparticles with shape and size control and their tunable peroxidase-like activity. *RSC Advances*, *5*(14), 10632–10640. https://doi.org/10.1039/c4ra15675g

Zhang, L., Wan, L., Chang, N., Liu, J., Duan, C., Zhou, Q., Li, X., & Wang, X. (2011). Removal of phosphate from water by activated carbon fiber loaded with lanthanum oxide. *Journal of Hazardous Materials*, *190*(1–3), 848–855. https://doi.org/10.1016/j.jhazmat.2011.04.021

Zhang, L., Zhou, Q., Liu, J., Chang, N., Wan, L., & Chen, J. (2012). Phosphate adsorption on lanthanum hydroxide-doped activated carbon fiber. *Chemical Engineering Journal*, *185–186*, 160–167. https://doi.org/10.1016/j.cej.2012.01.066

Zhang, S., Zhang, Y., Ding, J., Zhang, Z., Gao, C., Halimi, M., Demey, H., Yang, Z., & Yang, W. (2021). High phosphate removal using La(OH)3 loaded chitosan based composites and mechanistic study. *Journal of Environmental Sciences (China)*, *106*, 105–115. https://doi.org/10.1016/j.jes.2021.01.009

Zhang, Y., Zhou, F., Wang, W., Guo, H., Liu, M., Zhu, H., & Sun, H. (2020). Recyclable adsorbents based on Fe3O4 nanoparticles on lanthanum-modified montmorillonite for the efficient phosphate removal. *IET Nanobiotechnology*, *14*(6), 527–536. https://doi.org/10.1049/iet-nbt.2020.0012

Zheng, D., Yao, R., Sun, C., Zheng, Y., & Liu, C. (2021a). Highly Efficient Low-Concentration Phosphate Removal from Effluents by Recoverable La(OH)3/Foamed Nickel Adsorbent. *ACS Omega*, *6*(8), 5399–5407. https://doi.org/10.1021/acsomega.0c05489

Zheng, D., Yao, R., Sun, C., Zheng, Y., & Liu, C. (2021b). Highly Efficient Low-Concentration Phosphate Removal from Effluents by Recoverable La(OH)3/Foamed Nickel Adsorbent. *ACS Omega*, 5399–5407. https://doi.org/10.1021/acsomega.0c05489

Zhi, Y., Zhang, C., Hjorth, R., Baun, A., Duckworth, O. W., Call, D. F., Knappe, D. R. U., Jones, J. L., & Grieger, K. (2020). Emerging lanthanum (III)-containing materials for phosphate removal from water: A review towards future developments. *Environment International*, *145*, 106115. https://doi.org/10.1016/j.envint.2020.106115

Zhou, X., Chen, L., Wang, A., Ma, Y., Zhang, H., & Zhu, Y. (2015). Multifunctional fluorescent magnetic nanoparticles for lung cancer stem cells research. In *Colloids and Surfaces B: Biointerfaces* (Vol. 134). Elsevier B.V. https://doi.org/10.1016/j.colsurfb.2015.07.030

Zhu, X., Liu, Y., Qian, F., Zhou, C., Zhang, S., & Chen, J. (2014). Preparation of magnetic porous carbon from waste hydrochar by simultaneous activation and magnetization for tetracycline removal. *Bioresource Technology*, *154*, 209–214. https://doi.org/10.1016/j.biortech.2013.12.019

Zong, E., Huang, G., Liu, X., Lei, W., Jiang, S., Ma, Z., Wang, J., & Song, P. (2018). A lignin-based nano-adsorbent for superfast and highly selective removal of phosphate. *Journal of Materials Chemistry A*, *6*(21), 9971–9983. https://doi.org/10.1039/c8ta01449c

Appendix

Appendix I. Results of analysis for the optimum conditions

A. **Effect of pH on Phosphate removal**

pH	Co	Ce	qe(mg/g)	% Removal
1	100	3.738	28.8786	96.262
3	100	0.162	29.9514	99.838
5	100	0.066	29.9802	99.934
7	100	5.584	28.3248	94.416
9	100	11.004	26.6988	88.996
11	100	14.947	25.5159	85.053

B. **Effect of adsorbent dose on phosphate removal**

Dose(g/L)	**Co**	**Ce**	**qe(mg/g)**	% Removal
0.05	100	7.553	55.4682	92.447
0.1	100	5.949	28.2153	94.051
0.2	100	0.072	14.9892	99.928
0.4	100	0.058	7.4956	99.942
0.8	100	0.037	3.7486	99.963
1.0	100	0.019	2.9994	99.981

C. **Effect of contact time on phosphate removal**

Contact time(min)	**Co**	**Ce**	**qe(mg/g)**	**% Removal**
5	100	8.459	13.73115	91.541
15	100	2.337	14.64945	97.663
30	100	0.064	14.9904	99.936
60	100	0.178	14.9733	99.822
90	100	0.305	14.9543	99.695
120	100	0.771	14.8844	99.229

D. **Effect of initial concentration on phosphate removal**

Initial Conce(ppm)	Ce	qe(mg/g)	% Removal
1	0.004	0.1494	99.6
50	0.105	7.4842	99.79
100	1.988	14.7018	98.012
150	5.979	21.6032	96.014
200	14.679	27.7982	92.661
250	23.254	34.0119	90.698
300	37.028	39.4458	87.657

Appendix II. Experimental pictures during composite synthesis

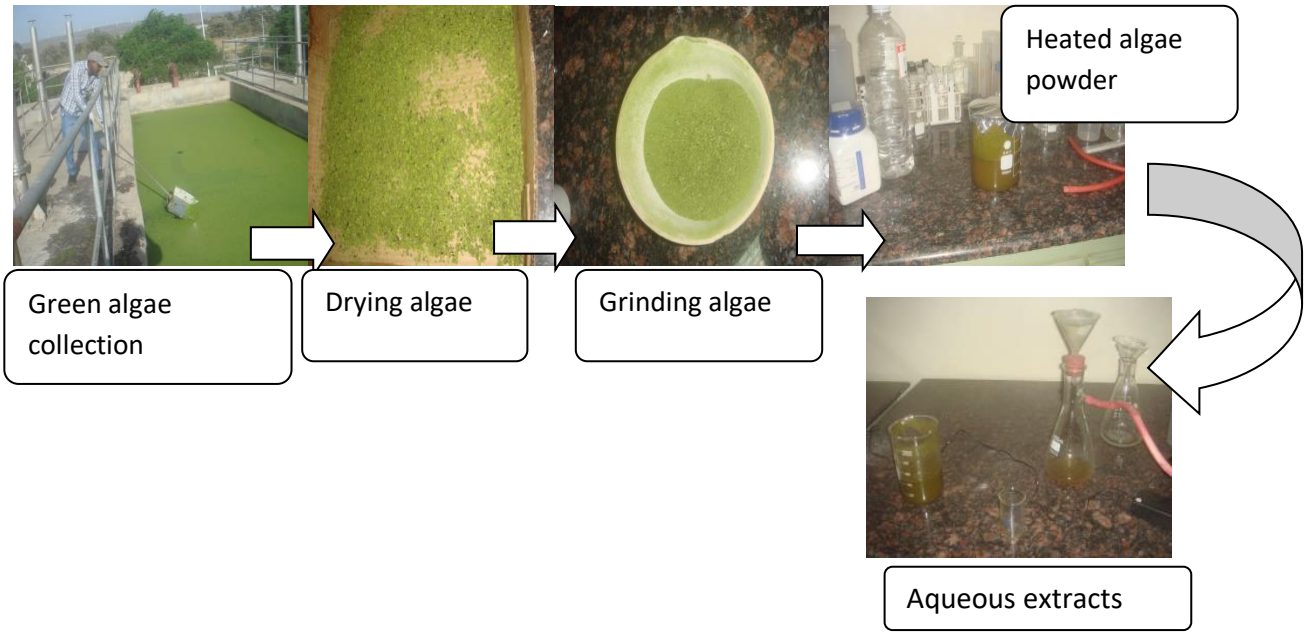

Figure II-1. Preparation of the reducing agent (green algae) from ASTU WWTP

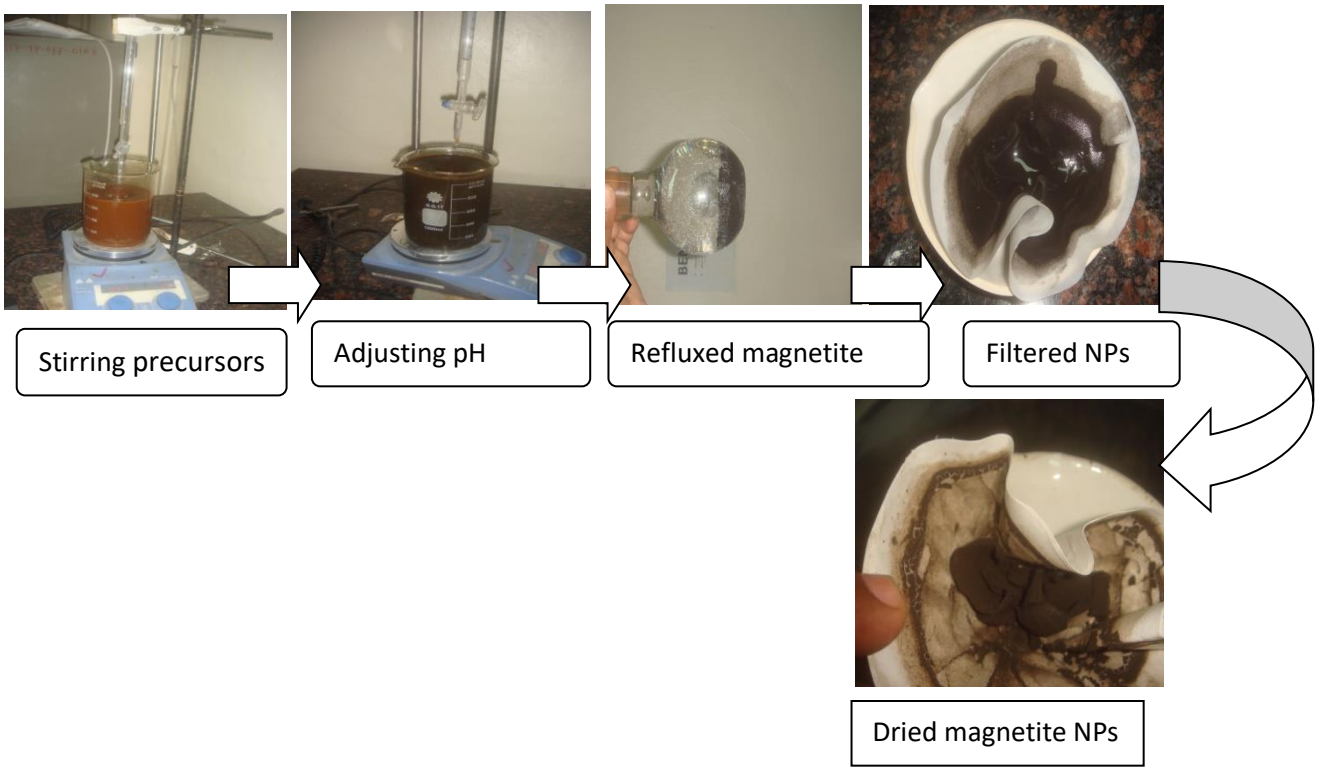

Figure II-2. Synthesis of magnetite nanoparticles

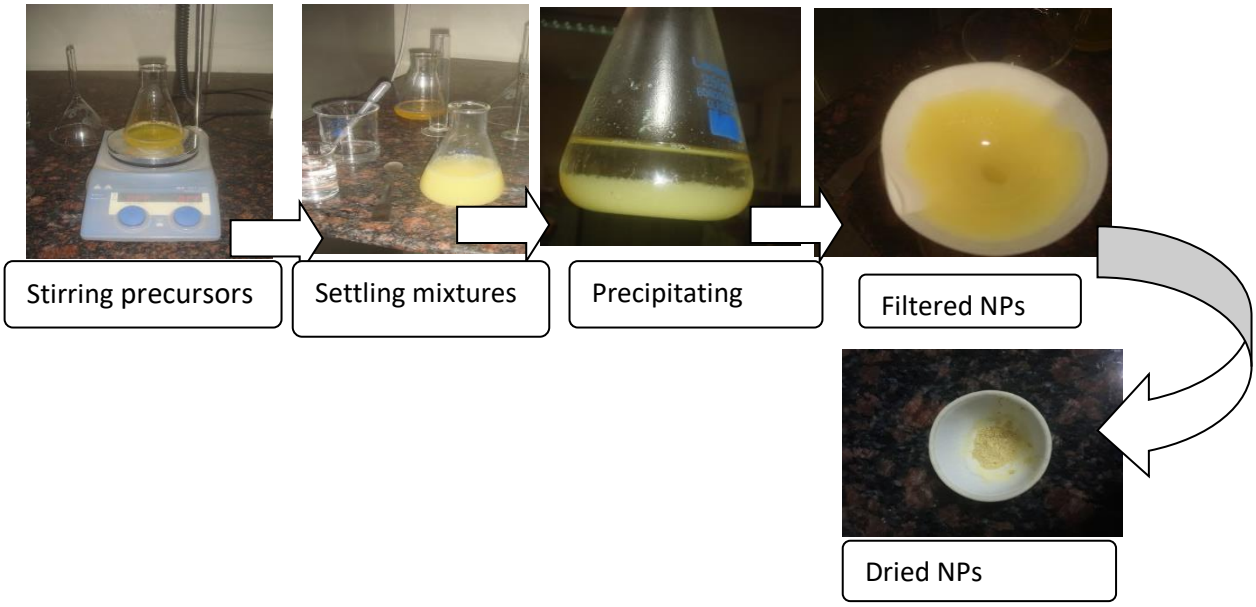

Figure II-3. Synthesis of $La(OH)_3$ nanoparticles

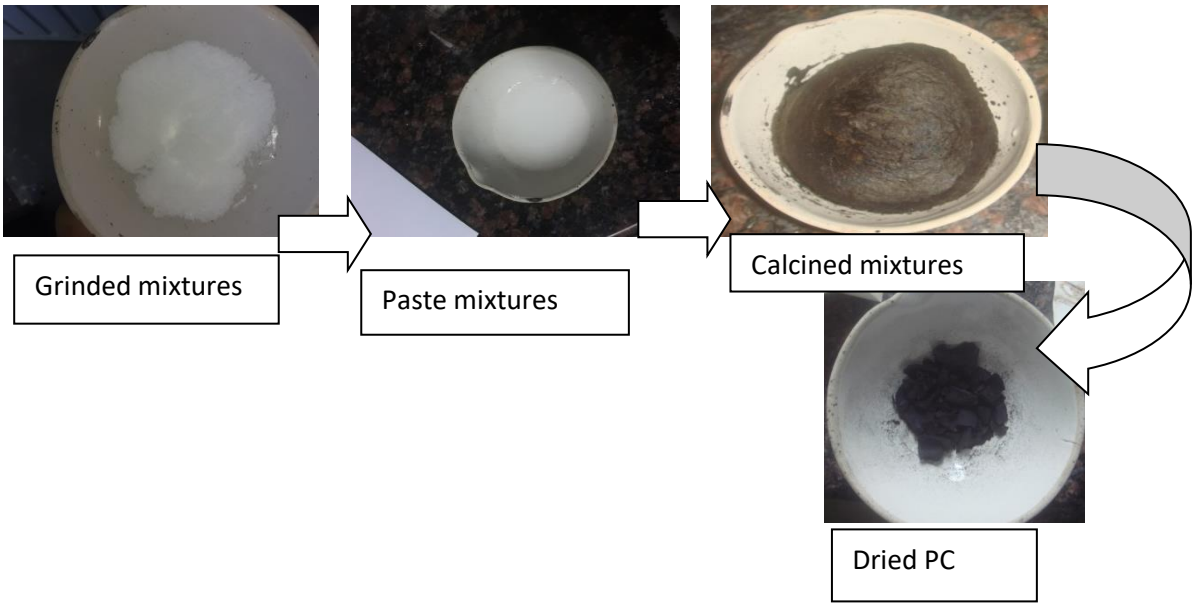

Figure II-4. Synthesis of porous carbon

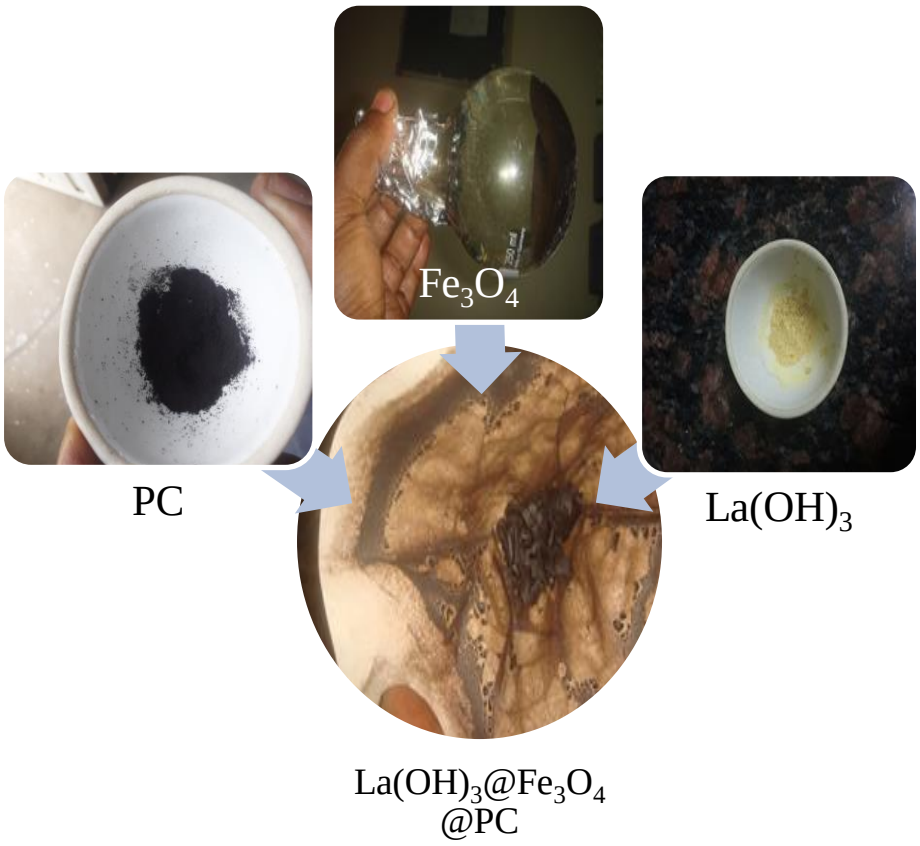

Figure II-5. Synthesis of the nanocomposite

Research Fund Acknowledgment

This work is financially supported by Adama Science and Technology University under the grant number ASTU/SM-R/616/22, Adama, Ethiopia